TEL AVIV UNIVERSITY

The Iby and Aladar Fleischman Faculty of Engineering

The Zandman-Slaner School of Graduate Studies

PEPTIDE-FUNCTIONALIZED SINGLE-WALLED CARBON NANOTUBES AS NEAR-INFRARED OPTICAL FINGERPRINTING SENSORS FOR HEAVY METAL-IONS

A thesis submitted toward the degree of

Master of Science in Biomedical Engineering

by

Gabriel Ernesto Petresky

March 2025

TEL AVIV UNIVERSITY

The Iby and Aladar Fleischman Faculty of Engineering

The Zandman-Slaner School of Graduate Studies

PEPTIDE-FUNCTIONALIZED SINGLE-WALLED CARBON NANOTUBES AS NEAR-INFRARED OPTICAL FINGERPRINTING SENSORS FOR HEAVY METAL-IONS

A thesis submitted toward the degree of

Master of Science in Biomedical Engineering

by

Gabriel Ernesto Petresky

This research was conducted in The Department of Biomedical Engineering Under the supervision of Prof. Gili Bisker

March 2025

Acknowledgments

First and foremost, I would like to thank my supervisor, Prof. Gili Bisker, for her ongoing guidance, encouragement, and support. She has pushed me professionally and believed in me and my research. She inspires professionalism and high work ethics, all with a smile and patience.

I would like to thank Dr. Verena Wulf for her direction, support, patience, and help throughout this process, and Michael Faran for his work on the ACFSA and for providing a great company during these years.

I would also like to thank Dr. Adi Hendler-Neumark for the initial training, support, and assistance during this process.

So many thanks to Shirel Kleiner for all the help and translations, for being an awesome company during these two years, and to everyone else in the Bisker Lab group, who created a friendly and pleasant environment to work in.

I would also like to acknowledge the Marian Gertner Institute for Medical Nano Systems for its support during my studies.

Finally, I would like to express my deepest gratitude to my family, Mario, Ester, and Gus, who supported and accompanied me from abroad, and to my partner Shira, who cruised along with me all this time and supported and endured me during all the research and writing.

Abstract

Heavy metals pose significant risks to human health and the environment. Their high toxicity arises from their ability to accumulate in living organisms, leading to severe health issues such as neurological disorders, kidney damage, and various forms of cancer. Inspired by natural metal-ion complexation sites formed by specific functional groups of the amino acids in enzymes and proteins, we propose a set of peptide-corona functionalized single-walled carbon nanotubes (SWCNTs), as a biocompatible, near-infrared fluorescence fingerprinting sensors for metal-ion identification. Each SWCNT-peptide sensor in this library features a unique sequence containing various amino acids for metal binding, revealing diverse optical response patterns to the various metal-ions evaluated. To enhance the diversity of the sensor library, we utilize different SWCNT chiralities and peptide coronae, which are additionally modified through photochemically induced chemical changes. These peptide-functionalized SWCNTs now comprise a suite of sensors that allow the identification of heavy metal-ions by analyzing fingerprint patterns. The ease of synthesis and peptide variability of the system facilitates the development of near-infrared fluorescent sensor arrays for a wide range of analytes and environmental conditions.

Publications

***Under review*, 2025**

Metal-ion Optical Fingerprinting Sensor Selection *via* an Analyte Classification and Feature Selection Algorithm

*Gabriel Petresky, Michael Faran, Verena Wulf, and Gili Bisker**

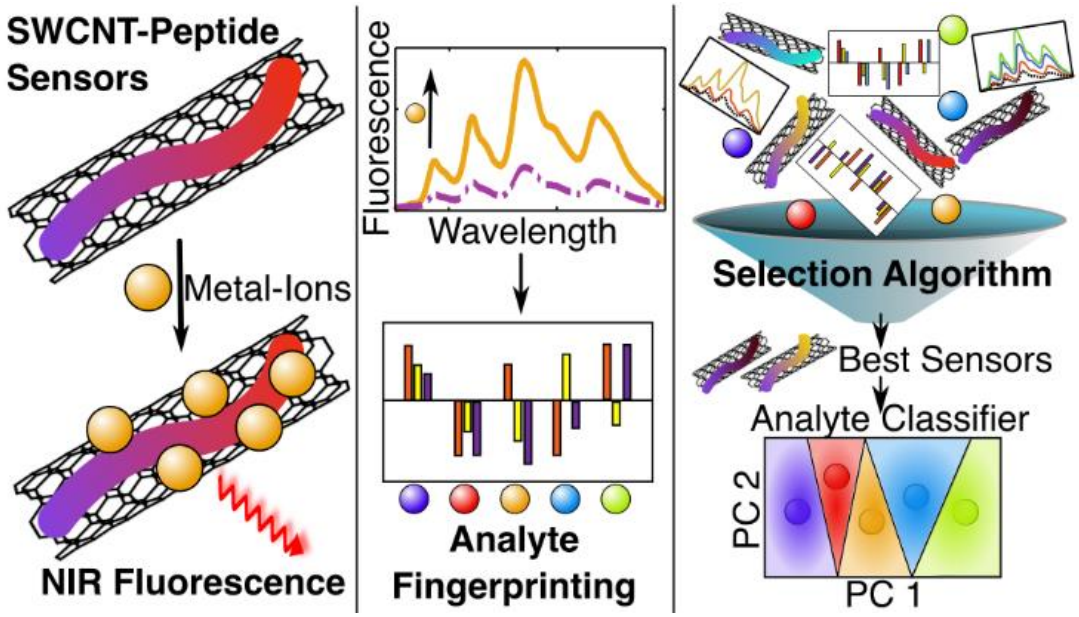

Petresky et al. present a system of synthesized peptide-functionalized single-walled carbon nanotubes (SWCNTs) as near-infrared, fluorescent, optical sensors for heavy metal-ions. By measuring the fluorescence modulation upon sensor-metal-ion interaction, they generate unique fingerprint patterns for each analyte. To optimize sensor selection for classification purposes, they developed the Analyte Classification and Feature Selection Algorithm (ACFSA), which processes the screening data of the fluorescence response of the resulting SWCNT-peptide sensors to the five analytes. Through iterative dimensionality reduction and rational sensor selection, the algorithm identified an optimal sensor set. The final output of ACFSA is thus an analyte classifier that enables analyte fingerprinting of heavy metal-ions using the selected sensors.

Table of Contents

List of Figures

1. Introduction

1.1 Biosensors

The development of biomedical or biochemical sensors relies on the ability to achieve specific and selective analyte recognition[1], Figure 1. Typically, molecular recognition for sensor development purposes is facilitated by macromolecules forming three-dimensional binding pockets, providing unique binding interaction with the analyte,[2] *e.g.*, *via* hydrogen bonds, π-π stacking, or electronic interactions for metal complexation.[3–7] Examples of natural macromolecular recognition units that are based on this principle include aptamers,[8] antibodies,[9] or the active site of enzymes.[10] Recent efforts in developing sensor recognition units have demonstrated that synthetic (bio)-macromolecules and polymers, which form a molecular corona around the surface of nanoparticle sensors, adapt a three-dimensional conformation that can also reveal high selectivity to certain analytes.[11–16]

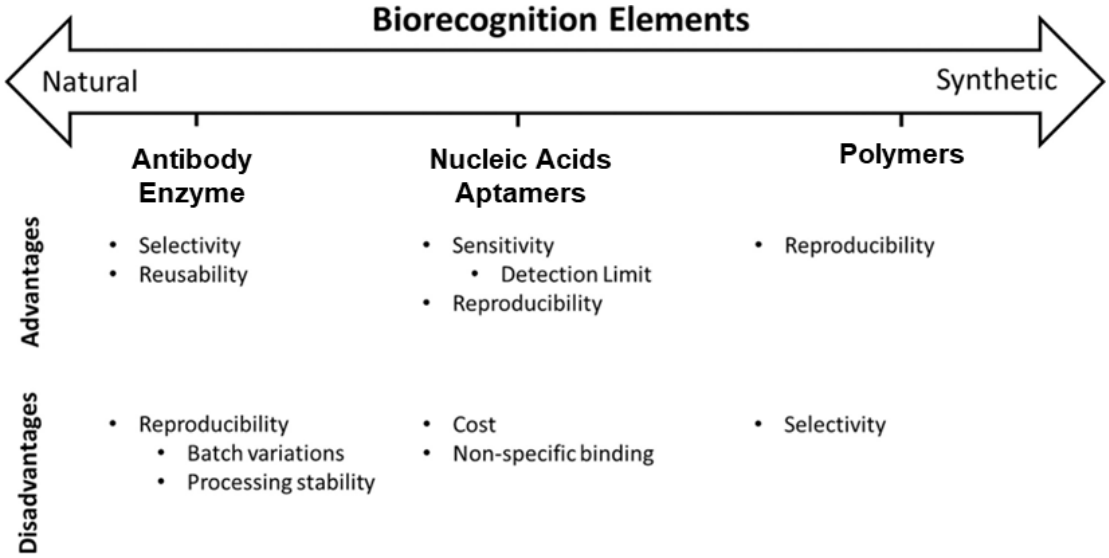

Figure 1. *Biorecognition elements and their advantages and disadvantages. Adapted with permission from.*[1]

A variety of polymers, as well as synthetic nucleic acid or peptide sequences, have been reported to form selective coronae for nanosensors,[17] with the advantage of reduced susceptibility to biodegradation and the potential greater stability against aging compared to natural biomolecules.[9] Further, using molecules without *a priori* inherent selectivity to the analytes allows for an extensive pool of potential sensor candidates for various compounds.[18–22] Despite recent efforts for computational elucidation of structure and functionality,[11,23–28] as well as advancements in directed evolution,[29–31] identifying a corona phase for selective sensing for a certain analyte still requires a

screening process involving time-consuming experimental work and data analysis. Although these sensors show high selectivity, achieving comparable effects to natural binding sites like aptamers or antibodies remains a challenge.[32] To improve the accuracy of a sensing platform, a combination of multiple sensors, each with a different corona, providing a fingerprint response for a specific analyte, can be employed instead of relying on a single sensor.[20,22] A fingerprint sensor typically consists of a set of several sensors that exhibit a distinct response pattern, such as optical or electronic signals, for each analyte from a defined library, thus providing the dataset to identify the analytes based on the response pattern.

1.2 Single-walled carbon nanotubes

One promising class of nanoparticles for various biomedical applications on the nanometer scale is single-walled carbon nanotubes (SWCNTs). The SWCNTs are comprised of sp2-hybridized carbon atoms, and can be described as rolled-up monolayer sheets of graphene.[33,34] The SWCNTs' diameter is in the order of 0.4-2 nm, while their length can extend from ~100 nm to several microns, providing a quasi-one-dimensional structure.[35] The sheet of graphene can roll up along different vectors, as described in Figure 2. The $\vec{a}\,1$ and $\vec{a}\,2$ represent different basis vectors in the hexagonal graphene lattice. The chirality of the SWCNT is defined as the linear combination of these two vectors, determining the roll-up direction of the sheet of graphene, which is described as:

$$\vec{Ch} = n * \vec{a}\,1 + m * \vec{a}\,2 \quad (1)$$

where n and m are positive integers.

The various chiralities are categorized into three distinct groups referred to as: "Zigzag" (Figure 2b), "Chiral" (Figure 2c), and "Armchair" (Figure 2d), for $m = 0$, $n \neq m$ and $n = m$, respectively.

The length of $|\vec{Ch}|$ is the circumference of the cylinder and the diameter of the SWCNT can be derived from:

$$D = \frac{|\vec{Ch}|}{\pi} = \frac{a}{\pi}\sqrt{n^2 + m^2 + nm} \quad (2)$$

where a is the length of the vectors $\vec{a}\,1$ and $\vec{a}\,2$.

The angle of the roll-up vector θ is the angle between $\vec{Ch}$ and $\vec{a}\,1$ and is described as:

$$\theta = cos^{-1}\left(\frac{2n + m}{2\sqrt{n^2 + m^2 + nm}}\right) \quad (3)$$

The roll-up vector of the SWCNT, defined by the chiral index (n, m), affects the density and energy of the electronic states[36], which determines the band gap between the conduction and valence bands, dictating the electrical, and optical properties. The $n = m$, "armchair" structure is metallic, $(n - m) = 3x$, $x \in \mathbb{N}$ is semi-metallic with a small band gap of roughly 1-100 meV whereas any other n, m combinations are semi-conductors[35,37] with a band gap that varies between 0.5-1 eV, which is negatively correlated with the diameter of the SWCNT.

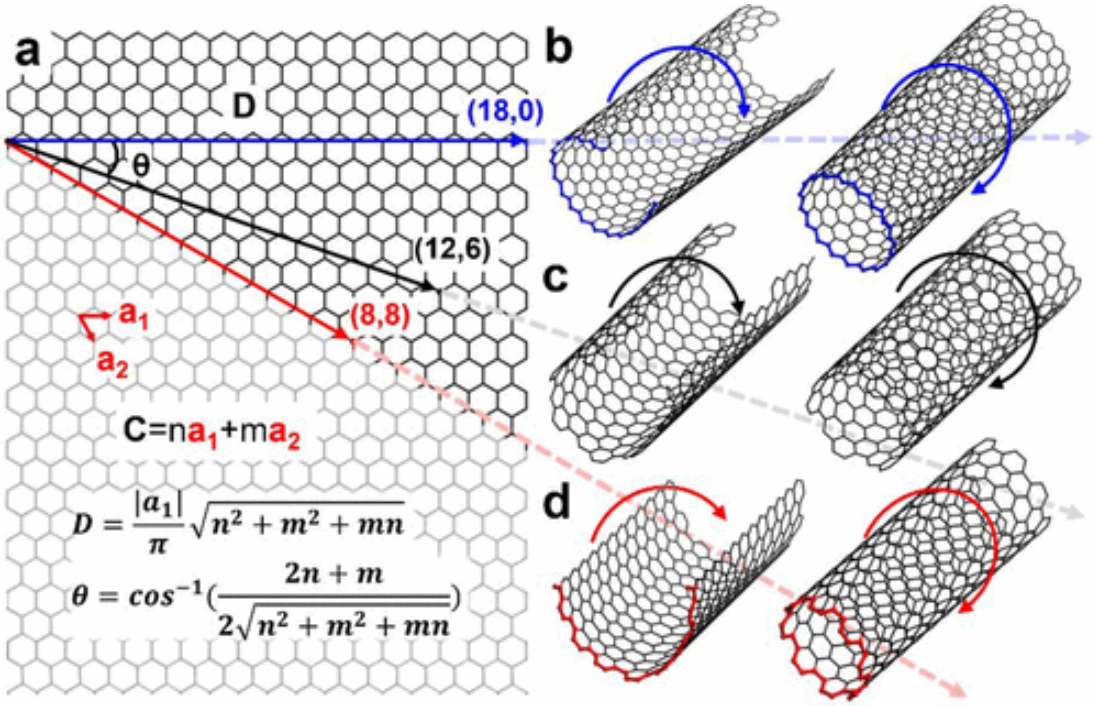

Figure 2. *Rolling vectors and chiralities. (a) Roll-up vector Ch of a graphene sheet determining the chirality of the SWCNTs, comprised of the linear combination of basis vectors a 1 and a 2 along with the chiral angle θ. Different SWCNT structures (b–d) dictated by the roll-up direction and the length of the vector. (b) "Zigzag" (c) "Chiral" and (d) "Armchair". Adapted with permission from* [38].

The fluorescence of the SWCNT is determined by the electronic band structure. An example of a typical band structure of a semiconducting SWCNT is described in Figure 3a. Light with energy $E22$ is absorbed by the SWCNT, exciting an electron from the valence band $V2$ to the conduction band $C2$, thus creating an electron-hole exciton with electrostatic Coulomb force. During relaxation, the electron decays to $C1$ due to lattice vibrations, and light with a lower energy $E11$ is emitted, typically in the NIR range.
The bandgap is dictated by the SWCNTs' chirality index (n, m), consequently different indices correspond to different excitation and emission wavelengths[37,39] (Figure 3b).

The fluorescence of the semiconducting SWCNTs is typically between 900 nm – 1600 nm, coinciding with the transparency window of biological samples (Figure 3c), where autofluorescence, absorption, and scattering are suppressed[40–44] which makes them particularly useful for intratissue sensing. Furthermore, SWCNTs do not photo-blink or photo-bleach[45] , therefore have a stable fluorescence over a long period of time.

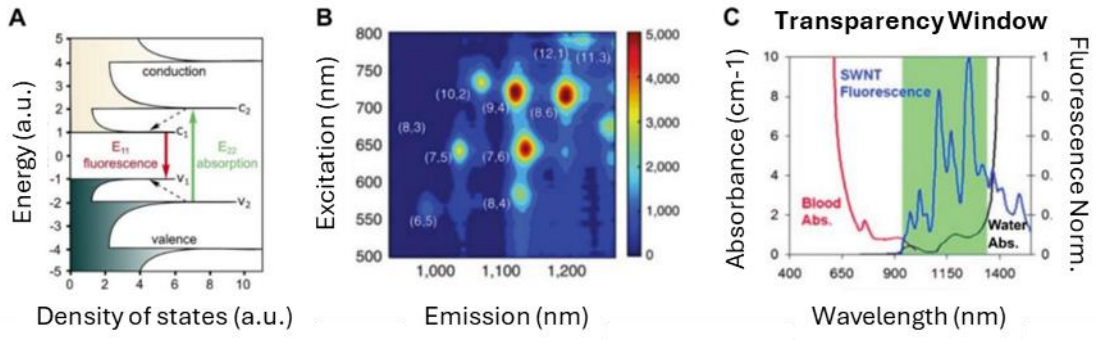

Figure 3. *Density of electronic states, SWCNT excitation emission map, transparency window. (a) Density of electronic states (DOS) of a semiconducting single-walled carbon nanotube structure. Solid arrows represent the excitation E22 (V2→C2) and emission E11 (C1→V1) transitions; dashed arrows indicate the non-radiative relaxation of electrons (in the conduction band) and holes (in the valence band) prior to emission. Adapted with permission from[36]. (b) Excitation–emission map of a PEGylated-functionalized SWCNT suspension with the different chiralities marked in white. Adapted with permission from[12]. (c) Biological Transparency window. SWCNTs (blue) fluoresce primarily in the near-infrared range (900–1600 nm). Blood (red) and water (black) absorbance spectra falls primarily in the visible regime and second infrared window, respectively. The range of minimal absorbance in biological samples in the near-infrared regime, has minimal interference with SWCNT fluorescence. Adapted with permission from[46] .*

Due to their fluorescence emission in the transparency window of biological tissue, the SWCNTs find widespread application in fluorescence sensing and imaging in biomedicine and bioengineering.[47–50]

1.3 SWCNTs functionalization and fluorescent modulation

The concept of functionalized SWCNTs as optical sensors has been developed for various applications, including the detection of enzymes,[51–56] RNA, lipids, and proteins,[12,57–60] small molecules,[58,61–66] pathogens,[18,22] and reactive oxygen species,[67–69] as well as multiple biomedical imaging and sensing applications.[42,44,70–76]

The SWCNTs' electronic and optical properties depend on their graphene lattice surface, which can be maintained by purely non-covalent functionalization with a corona phase, or modified covalently via the introduction of defect sites.[36] The former fully maintains the sp^2 lattice structure and is typically performed using macromolecules such as single-stranded DNA,[77–79] surfactants,[80–82] amphiphilic polymers,[54,83–86] proteins,[87–89] and suitable peptides[18,90] that can bind the graphene lattice of the SWCNTs via hydrophobic interactions or π-π stacking (Figure 4).

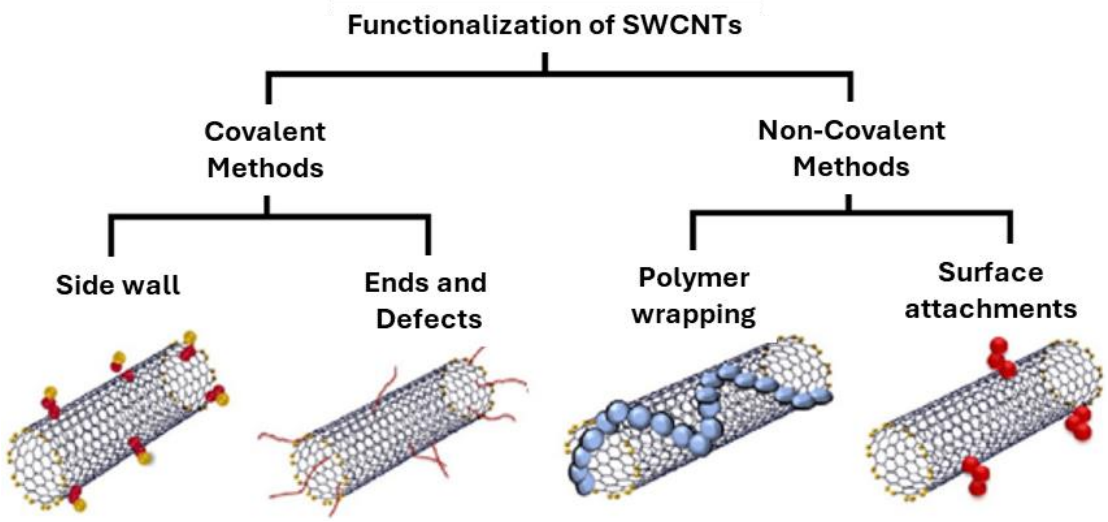

Figure 4*. Classification of SWCNTs functionalization methods. Adapted with permission from*[91].

When an analyte binds to the corona phase of the SWCNTs, it induces changes in the SWCNT dielectric environment, either directly or through additional structural modification in the corona phase of the SWCNTs. These changes can be manifested in modulations of the SWCNTs' fluorescence emission wavelength and/or intensity.[36,72,92] Furthermore, studies have shown that individual (*n*,*m*)-chiralities within a SWCNT sample can exhibit different fluorescence responses to a specific analyte, even when functionalized with the same corona phase.[93,94] This effect is attributed to the differences in the diameters and curvatures of the various SWCNT chiralities, which can affect the structure of the formed three-dimensional corona, thereby enhancing or hindering analyte binding. Thus, the fluorescence modulations due to changes in the polarity and dielectric environment of the SWCNTs have been found to be chirality-dependent.[95–97] Consequently, functionalizing a sample of SWCNTs containing different chiralities results in a mixture of individual sensors, which can be easily

resolved optically by monitoring their specific excitation and emission wavelength, a unique advantage of using SWCNTs compared to other optical nanosensors.

1.4 Peptide-SWCNTs metal-ion sensors

The development of transition metal-ion sensors is crucial due to the significant effects of these metals on the environment and human health.[98,99] Elevated levels of metal-ions such as lead, copper, or chrome in living organisms can lead to enzymatic dysfunction and contribute to diseases like cancer and neurodegenerative disorders.[100,101] Most metal-ion detectors operate by complexing metal ions with molecules or polymers containing chelating groups or DNA-aptamers that form metal-specific binding sites.[5,102,103] However, the high complexity of many metal-binding molecules poses significant challenges to their synthesis.[5,103]

We take advantage of the SWCNTs-peptide properties to tackle this issue. In a previous study, it was shown that SWCNTs functionalized with a melanin-like material, synthesized from fluorenylmethoxycarbonyl (Fmoc)-protected tyrosine, had metal-ion interacting properties.[3] After functionalizing the SWCNTs with the amino acid, the suspension underwent an enzymatic oxidative polymerization by tyrosinase, resulting in a melanin-like polymer containing quinone and catechol groups in the corona phase of the SWCNTs. These functional groups are known for their ability to chelate divalent metal-ions.[104] While it was demonstrated that these sensors could interact with metal ions, resulting in an optical response, the different metals could not be distinguished using that approach.[3]

In proteins and enzymes with metal-ion reaction centers, metal-binding sides are formed by the interplay of different amino acids, each with specific side-chain functional groups, such as amine groups in lysine or the carboxyl groups in glutamic acid.[105,106] Thus, SWCNTs functionalized with a corona phase of peptides composed of different amino acids could potentially achieve a more selective metal-ion recognition by generating distinct fluorescence modulation for each sensor-analyte pair (Figure 5). Further, variations in the peptide sequences, chemical modification of the corona phase, and the use of different SWCNT chiralities would enable the construction of an extensive library of metal-ion sensors, from which a selection of a small sensor set for a fingerprinting platform could be identified.

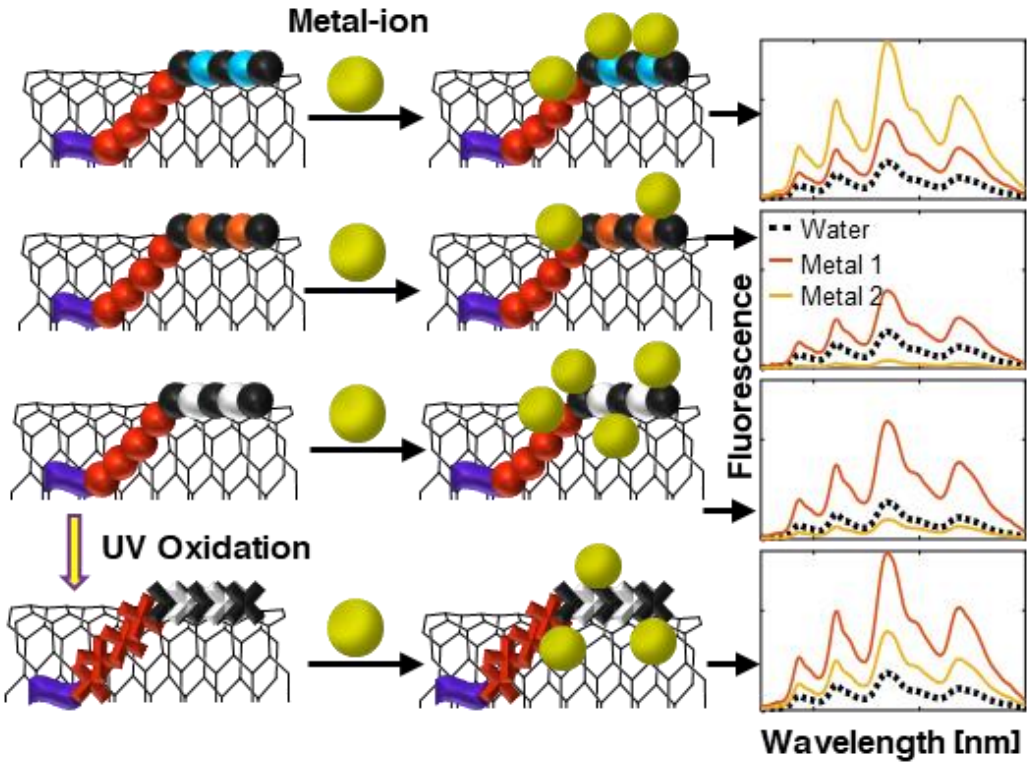

Figure 5. *Peptide functionalized SWCNTs metal-ion fluorescence response. SWCNTs functionalized with different peptides, with or without oxidative modifications, interact with metal-ions and generate a distinctive fluorescent modulation response.*

Research goal

This work sets out to create fluorescent SWCNTs functionalized with diverse peptide corona phases as an optical fingerprinting sensor platform for transition metal-ions, namely: copper (Cu^{2+}), nickel (Ni^{2+}), chromium (Cr^{3+}), lead (Pb^{2+}), and mercury (Hg^{2+}). We aim to exploit the variability of the SWCNTs-amino-acids/metal-ions interactions to create an analyte identifier based on the fluorescence response patterns.

The main motivation is to generate a biocompatible, near-infrared fluorescent sensor set that can be utilized to produce fingerprinting patterns of the analytes of interest and prove this concept on heavy metal-ions.

For this purpose, the SWCNTs were suspended with a set of five Fmoc-peptides having the sequence Fmoc-FFFFYXYXY, each consisting of a phenylalanine chain (FFFF) and an alternating sequence of tyrosine (Y) and a variable amino acid (X). While the Fmoc-FFFF chain facilitates binding to the SWCNTs by π-π stacking, the alternating sequence YXYXY contains tyrosine, to provide the same functionality exploited in previous work,[3] and functional groups such as guanidino, carboxyl, amine, and thiol, provided by the varying amino acids (arginine, glutamic acid, lysine, cysteine), adding glycine as an amino acid without a complex side chain. These groups allow for distinct metal-ion complexation and interactions.

To further diversify the peptide library, the SWCNT-Fmoc-peptides underwent photochemical oxidization, resulting in additional variations in the corona phase, like tyrosine dimerization and new functional groups through oxidation.

We tested the suspension stability, oxidation results, optical characteristics of the new sensors, and fluorescent modulation upon metal-ion integration.

Consequently, this process yielded ten SWCNT-Fmoc-peptide sensors, including the oxidized and non-oxidized forms, where each sensor sample contained a mixture of SWCNT chiralities. By monitoring three chiralities in each SWCNT-peptide sample at their respective fluorescence excitation and emission wavelengths, we established a library of thirty potential sensors that generated a fingerprinting dataset for analyte identification (Figure 6).

The best sensor, identified as having the highest variance between the analytes by the Analyte Classification and Feature Selection Algorithm (ACFSA) developed by

Michael Faran, was selected to test functionality in mineral water and serum as well as a general limit of detection.

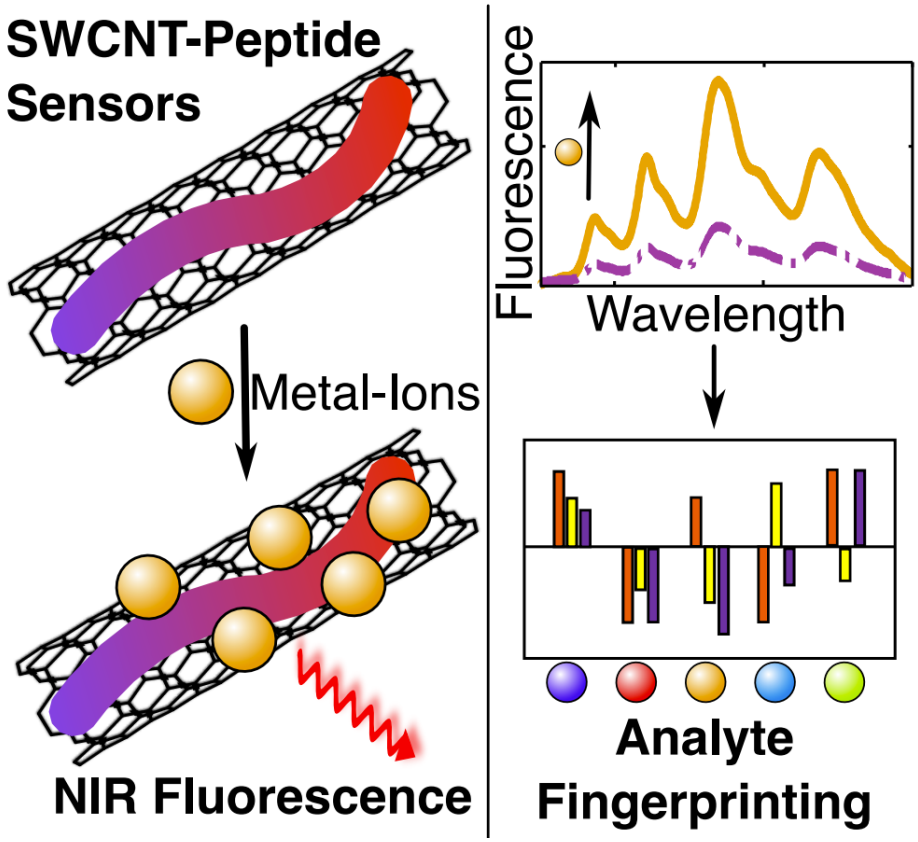

Figure 6. *Fingerprint generation from metal-ion Peptide-SWCNTs interactions. Peptide functionalized SWCNTs interact with metal-ions and generate a change in the sensor's fluorescence, the library generated from these changes fingerprints the analytes.*

2. Methods

2.1 Suspension of SWCNT with Fmoc-peptides.

15 mg of Fmoc-peptides (ABclonal) were dissolved in 1 mL of water. For complete peptide dissolution, Fmoc-FFFFYEYEY and Fmoc-FFFFYGYGY required the addition of sodium hydroxide (0.5 M, approximately 50 µL). Fmoc-FFFFYRYRY was first dissolved in 50 µL of DMSO, then 950 µL of distilled water was added, whereas Fmoc-FFFFYCYCY was dissolved in 200 µL of DMSO, and then 800 µL of water and 20 µL of 0.5 M NaOH were added to complete dissolution. Fmoc-FFFFYKYKY was dissolved in water without any additions. Subsequently, 2 mg of high-pressure carbon monoxide (HiPCO) SWCNTs (NanoIntegris) were suspended in 1 mL of the 15 mg mL^{-1} Fmoc-peptide solution using direct tip sonication on ice for 60 minutes (4 W, QSonica Q125). After sonication, the suspension was centrifuged twice for 1.5 h at 21,130 rcf (Eppendorf 5424 R), and 80% of the supernatant was recovered to separate the individually suspended SWCNTs from aggregates. The SWCNT-Fmoc-peptide suspensions were then filtered via a centrifugal filter (Amicon, MWCO 100 kDa) and washed three times with ddH_2O to remove excess Fmoc-peptides, salts, and DMSO, and equilibrate the pH for all samples. The concentrations of the SWCNT-Fmoc-peptides suspension were determined using the extinction coefficient $\varepsilon_{632\,nm}$=0.036 L mg^{-1} cm^{-1},[62] and found to be between 100 mg L^{-1} and 300 mg L^{-1}.
For SWCNT-SDS, the process is similar but instead of peptides, a solution of 2% SDS (Bio-Lab ltd.) was used for sonication, washing and resuspending.

2.2 UV Oxidation.

A total of 10 mL of each SWCNT-peptide suspension at a concentration of 50 mg L^{-1} was transferred into an 8 cm diameter glass open petri dish. The suspensions were subjected to λ = 254 nm UV irradiation (Vilver, 6W) from above at 4 cm distance for 90 min while magnetic stirring.

2.3 Absorption and fluorescence spectroscopy of peptide oxidation.

The SWCNT-peptide fluorescence and absorption measurements following the peptide oxidation were recorded using a plate reader (Fusion Optics Reader Platform SPARK, Tecan). Fluorescence measurements were performed with two different filter sets,

λ_{ex} = 280 nm and λ_{em} = 300–600 nm; and λ_{ex} = 320 nm and λ_{em} = 350–600 nm. To show the coloration of the Fmoc-peptides before and after oxidation, the SWCNT-peptides were lyophilized, and the peptides were then resuspended in DMSO while the SWCNTs remained in the precipitate.

2.4 NIR fluorescence spectroscopy of SWCNTs.

Fluorescence emission spectra were recorded in a 96-well plate mounted on an inverted microscope (Olympus IX73). A super-continuum white light laser (NKT-photonics, Super-K Extreme) with a bandwidth filter (NKT-photonics, Super-K varia, $\Delta\lambda$ = 20 nm) was coupled into the microscope as the excitation source with a laser intensity of 20 mW. Fluorescence emission was spectrally resolved using a spectrograph (Spectra Pro HRS-300, Teledyne Princeton Instruments) with a slit-width of 500 µm and a grating (150 g mm^{-1}). The fluorescence intensity spectrum was recorded by an InGaAs-detector (PylonIR, Teledyne Princeton Instruments). Excitation-emission maps were recorded using an excitation wavelength range of 500 nm to 840 nm in 2 nm steps.

2.5 NIR fluorescence response to metal-ions.

Copper(II) Chloride ($CuCl_2$), Nickel(II) Chloride ($NiCl_2$), Chrome(III) Chloride ($CrCl_3$), Lead(II) Chloride ($PbCl_2$), and Mercury(II) Chloride ($HgCl_2$) were purchased from Sigma-Aldrich. For the measurements, aliquots of 147 µL of 1 mg L^{-1} SWCNT-peptides in water were placed in a 96-well plate and treated with 3 µL metal-ion solution in water to obtain a final metal-ion concentration of 300 µM or with 3 µL water as a control. The NIR-fluorescence emission spectra of the SWCNT-peptides were measured after an incubation time of 15 min at an excitation wavelength of λ=570 nm, 660 nm, and 730 nm, with an intensity of around 20 mW, corresponding to the excitation resonance of the (6,5), (7,5), and (9,4) chiralities of the SWCNTs, respectively.

2.6 Raman spectroscopy:

Raman spectra were acquired using a confocal micro-Raman (PL) spectrometer (LabRam HR Evolution). Samples of 20 mg L^{-1} of the ten SWCNTs-peptide suspensions were placed on a 1 cm path cuvette and excited with a 532 nm laser.

Measurements were taken with a ×100 objective lens at a laser power of 100 mW for 3 seconds. Water was used as blank.

2.7 NIR fluorescence response in serum:

Aliquots of 147 µL solution containing 5% fetal bovine serum (FBS, Biowest, USA) and 1 mg L^{-1} of SWCNT-Gly sensor were mixed with 3 µL of 30 mM metal-ion chlorides, Cu^{2+}, Ni^{2+}, Cr^{3+}, Pb^{2+}, and Hg^{2+}.

2.8 NIR fluorescence response in mineral water:

Aliquots of 147 µL solution of commercial mineral water (Neviot, Israel) and 1 mg L^{-1} of SWCNT-Gly sensor were mixed with 3 µL of 15 mM metal-ion chlorides, Cu^{2+}, Ni^{2+}, Cr^{3+}, Pb^{2+}, and Hg^{2+}.

2.9 Sensor response analysis:

The peaks of the respective chiralities were fitted with a Lorentzian distribution function, and the relative intensity changes of the sensors in response to the different metal analytes were determined (Matlab).

3. Results and discussion:

3.1 Peptide design and sensor optical properties

To explore the potential of fluorenylmethoxycarbonyl (Fmoc)-protected peptides as effective corona phases of SWCNTs for transition metal-ion sensing, we utilized the peptide sequence Fmoc-FFFFYXYXY, consisting of phenylalanine (Phe, F), tyrosine (Tyr, Y), and a variable amino acid (X), which is either arginine (Arg, R), glutamic acid (Glu, E), lysine (Lys, K), cysteine (Cys, C) or glycine (Gly, G) (Figure 7). These peptides were designed to provide functional groups through tyrosine and the variable amino acids, *i.e.*, guanidine-, amine-, carboxyl-, hydroxyl-, and thiol-groups, to form a corona phase that can complex metal-ions.[3,105,107] Glycine was included as an amino acid without an additional side chain. Further, the Fmoc-FFFF-tail facilitated the attachment of the Fmoc-peptide to the SWCNTs and their dispersion in water. Notably, without the additional phenylalanine-chain, the Fmoc-peptides showed very low efficiency as SWCNT dispersants.

We refer from now on to these sensors as SWCNTs-XXX where XXX is the name of the variable amino acid in the chain, we add a suffix OX if it was exposed to the oxidative process.

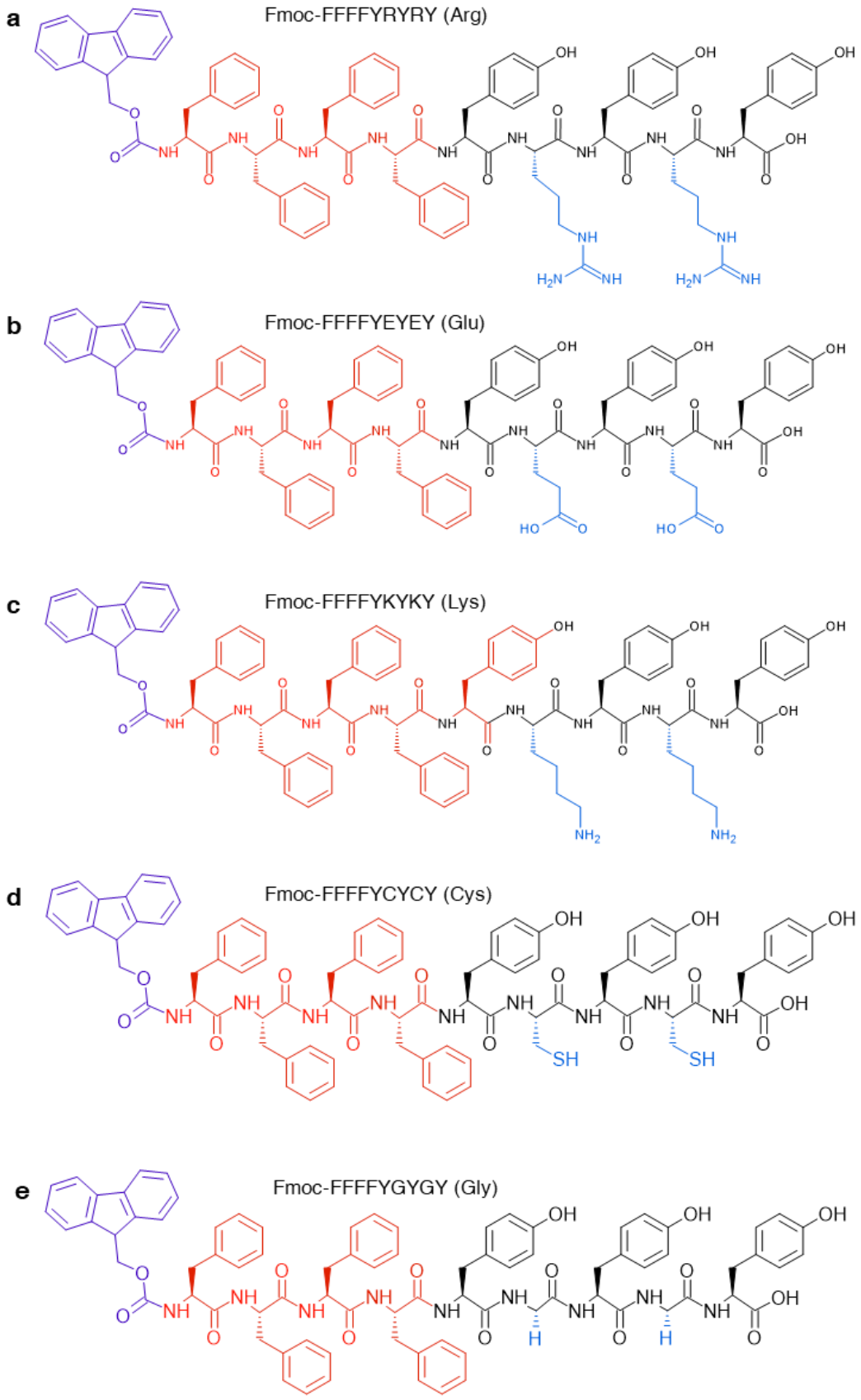

***Figure 7**: Molecular structures of the Fmoc-peptides. Fmoc-group (purple), phenylalanine (F) chain (red), tyrosine (black), variable amino acid (blue). a) Fmoc-FFFFYRYRY (R: Arginine),*

b) Fmoc-FFFFYEYEY (E: Glutamic acid), c) Fmoc-FFFFYKYKY (K: Lysine), d) Fmoc-FFFFYCYCY (C: Cysteine), e) Fmoc-FFFFYGYGY (G: Glycine).

Figure 8a-e, shows the absorption spectra of the Fmoc-peptide functionalized SWCNTs (SWCNT-Arg, SWCNT-Glu, SWCNT-Lys, SWCNT-Cys, and SWCNT-Gly).

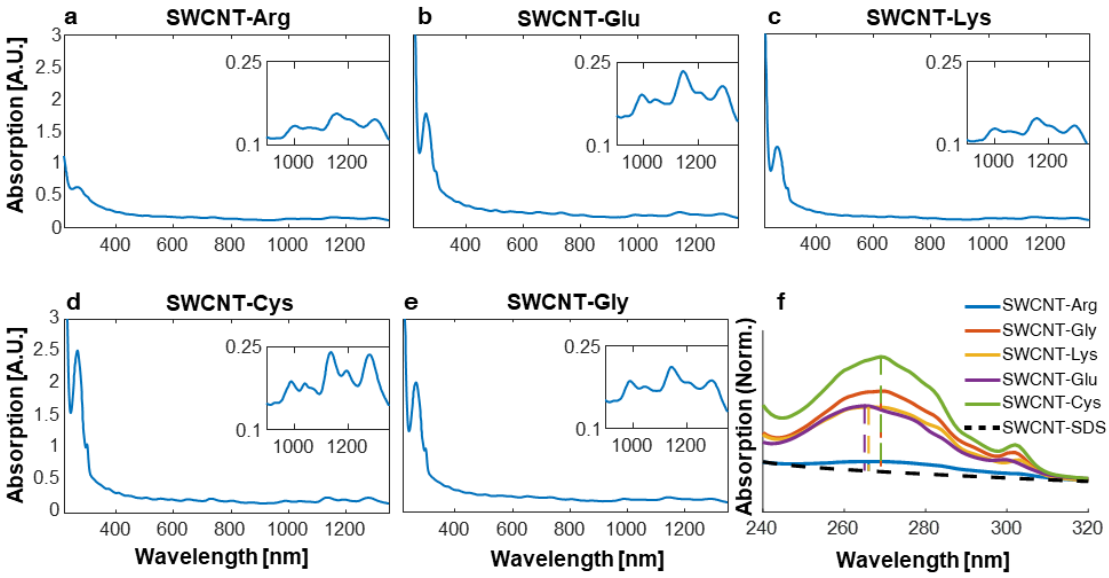

***Figure 8**: Absorption spectra of the SWCNT-peptide suspensions diluted 1:20 in water. a) SWCNT-Arg, b) SWCNT-Glu, c) SWCNT-Lys, d) SWCNT-Cys, e) SWCNT-Gly. Insets: NIR absorption of the SWCNTs. f) Comparison of the Fmoc-absorption peaks at 270 nm at normalized concentration of carbon nanotubes of SWCNT-Arg (light blue), SWCNT-Glu (orange), SWCNT-Lys (yellow), SWCNT-Cys (purple), and SWCNT-Gly (green).*

For all Fmoc-peptides, defined peaks corresponding to the SWCNTs' E_{11} and E_{22} electronic transitions are clearly observed between 900 and 1300 nm (Figure 8a-e, insets), indicating successful suspensions. Additionally, the peak at around 270 nm corresponds to the Fmoc-group, confirming the presence of the Fmoc-peptides in the corona phase of the SWCNTs after filtering the samples from excess Fmoc-peptides. However, the SWCNT surface coverage by the Fmoc-peptides varies depending on the peptide sequence, as evident from the different UV absorption of the Fmoc-group (Figure 8f), the ratios, against a SWCNTs-SDS background, which do not have Fmoc or aromatic groups that absorb in this range, and, normalized at 632 nm to compensate for SWCNT concentration variations, and compared against SWCNT-Arg are: SWCNT-Arg: 1.0, SWCNT-Gly: 8.5, SWCNT-Lys: 6.7, SWCNT-Glu: 6.8, SWCNT-

Cys: 12.0. SWCNT-Arg, for example, contains the least amount of Fmoc-peptide per milligram of SWCNTs, while SWCNT-Cys has the highest amount. These variations in the SWCNT surface coverage suggest different affinities of each peptide to the SWCNT surface and potential electrostatic repulsion between the Fmoc-peptides molecules. Nevertheless, all five SWCNT-peptide suspensions were stable in water for several months at concentrations of 50 mg L^{-1}.

HiPCO SWCNTs combine several different chiralities within a single SWCNT sample, with each chirality characterized by its band gap energy, resulting in distinct fluorescence excitation and emission wavelengths. Further, it has been observed that each chirality can exhibit a distinct fluorescence response to analytes binding to their corona, influenced by the different curvature and surface coverage of the SWCNTs.[35,93,96] Consequently, every SWCNT-chirality in our SWCNT-peptide sample can be considered an independent sensor. For our measurements, we selected three different chiralities, namely the (6,5), (7,5), and (9,4) chiralities, which are excited at λ_{ex} = 570 nm, 660 nm, and 730 nm, respectively, and show fluorescence emission at around λ_{em} = 995 nm, 1050 nm, and 1130 nm, respectively. This selection of three wavelengths was made to allow for maximal spectral separation and minimal overlap, ensuring clear and reliable fluorescence responses across the chosen chiralities. The complete excitation-emission maps of all five sensors are shown in Figure 9.

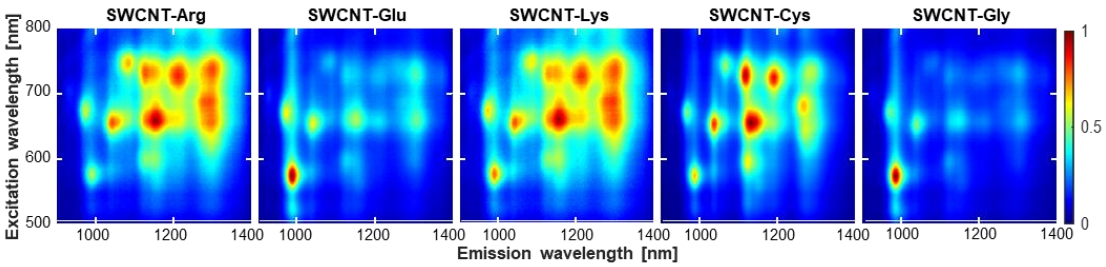

***Figure 9**. Excitation emission maps of the SWCNT-peptide suspensions.*

We select SWCNT-Cys as an example. In Figure 10a, we showcase the resulting fluorescence spectra when exciting at the corresponding wavelengths, λ_{ex} = 570 nm, 660 nm, and 730 nm. The peaks analyzed are marked with arrows. Figure 10b shows the resulting full excitation-emission map, with the chiralities measured marked with black circles.

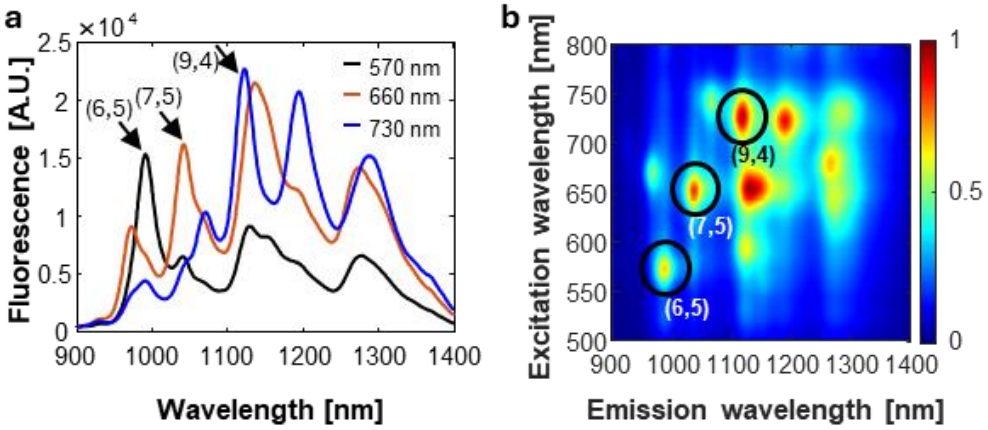

Figure 10. *Fluorescence emission spectra of three chiralities and excitation emission map of SWCNT-Cys. a) Fluorescence emission spectra of SWCNT-Cys at three different excitation wavelengths: 570 nm (black), 660 nm (orange), and 730 nm (blue). Emission peaks of the three chiralities measured at these excitation wavelengths are marked with arrows corresponding to the (6,5), (7,5), and (9,4) chiralities, respectively. b) Normalized excitation-emission map of SWCNT-Cys. The three chiralities shown in b) are highlighted in circles.*

3.2 Sensor oxidation

To further extend our SWCNT-peptide sensor library, we chose to photochemically oxidize the tyrosine-containing peptide corona of the SWCNTs *via* UV irradiation. Tyrosine and tyrosine-containing peptides that undergo photochemical oxidation are known to form dimers of dityrosine and, in some cases, to further oxidize to melanin-like derivatives.[108,109] The resulting variations of the SWCNT corona are expected to affect analyte recognition,[12] thereby, we effectively expand our initial sensor library. In a previous study, Fmoc-tyrosine that underwent enzymatic oxidative polymerization *via* tyrosinase to a melanin-like material demonstrated improved stability as a SWCNT dispersant and enhanced performance in metal sensing attributed to the formation of metal-scavenging functional groups like catechols and quinones.[3] Nevertheless, due to the more complex peptide structure in the current study, we chose photochemical oxidation instead of enzymatic oxidation.

For the oxidation of the Fmoc-peptide corona of the SWCNTs, we exposed the suspensions to UV light (254 nm) and monitored the reaction via absorption and fluorescence spectroscopy. Compared to the absorption of SWCNT-peptides, the absorption spectra of the oxidized suspension after UV irradiation, the oxidated sensors,

referred to as SWCNT-“X-peptide”-Ox, showed a slight increase in absorption below 500 nm (Figure 11 column a), consistent with the observable browning of the Fmoc-peptide solution due to tyrosine oxidation also reported in previous works.[3,110] Additionally, the fluorescence emission of the peptides in the SWCNT-peptide suspension before and after UV-oxidation exhibited a decrease in the fluorescence intensity of tyrosine (λ_{ex} = 280 nm, λ_{em} = 320 nm) and an increase in the fluorescence intensity at λ_{em} = 420 nm, associated with the formation of dityrosine and its oxidized derivatives (Figure 11, columns b and c).[109] These results were obtained for most of the suspensions, for SWCNT-Arg, absorption increase and coloration were hardly observed, probably due to a lower amount of Fmoc-peptides in the corona phase of this particular sensor compared to the other sensors (Figure 11 a and d, first line). SWCNT precipitation in DMSO (Figure 11 column d) shows the browning of the peptides remaining in the solution.

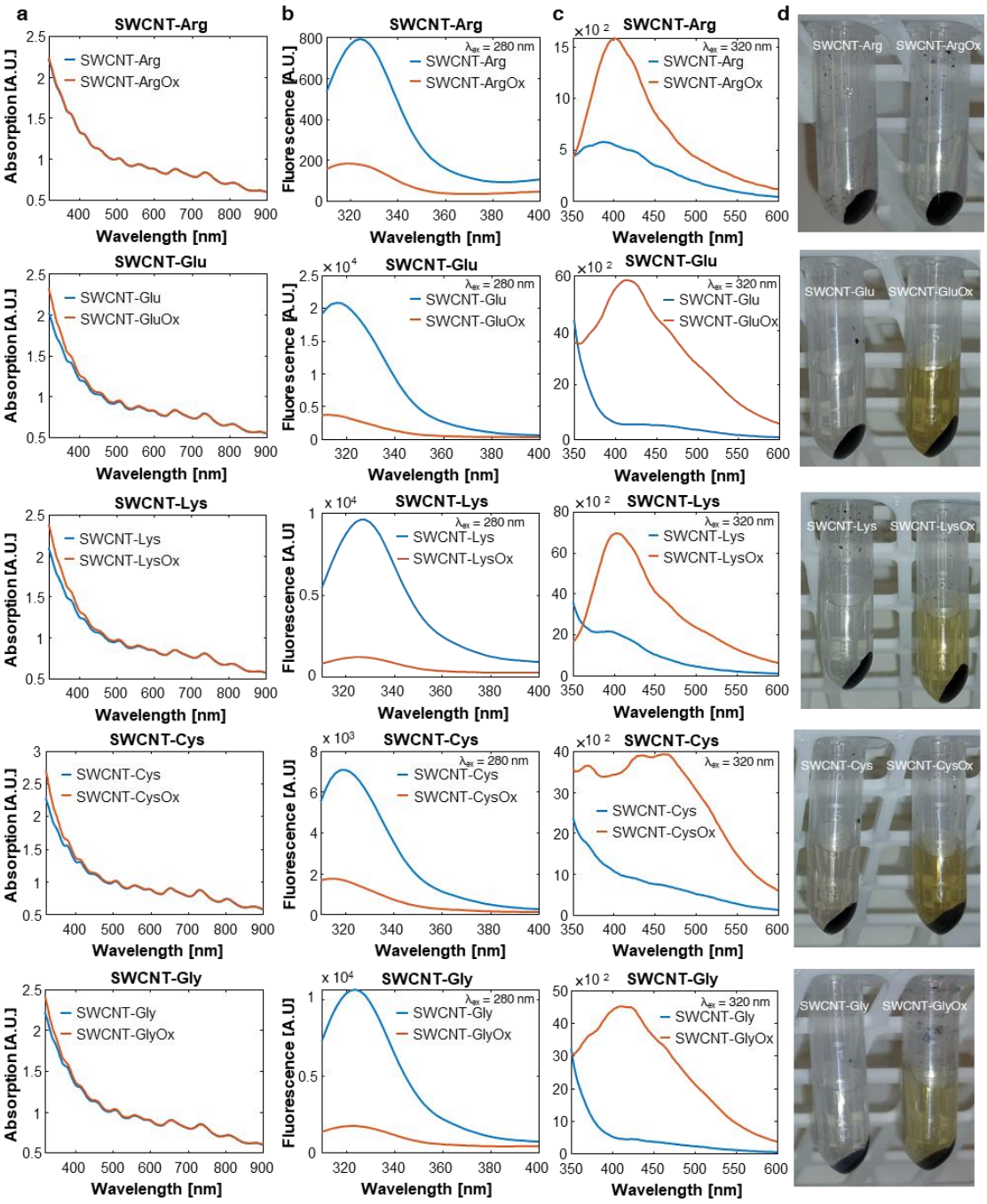

Figure 11. *Absorption and fluorescence spectra of the SWCNT-peptides before and after oxidation. a) Absorption spectra of the SWCNT-peptide suspensions before (blue) and after (orange) oxidation. b) Decrease in fluorescence intensity under 280 nm excitation before (blue) and after (orange) oxidation. c) Increase in fluorescence intensity under 320 nm excitation before (blue) and after (orange) oxidation. d) Coloration of the peptides extracted with DMSO from the SWCNT-peptide suspension before (left) and after (right) oxidation. From top to bottom: SWCNT-Arg, SWCNT-Glu, SWCNT-Lys, SWCNT-Cys, SWCNT-Gly.*

The ten complete excitation-emission maps, shown in Figure 12 for ease of comparison, include the original sensors (Figure 12 first row) and, the oxidated sensors,

referred as SWCNT-“X-peptide”-Ox, (Figure 12, second row), confirm that the fluorescence properties of the SWCNTs are still present after UV oxidation.

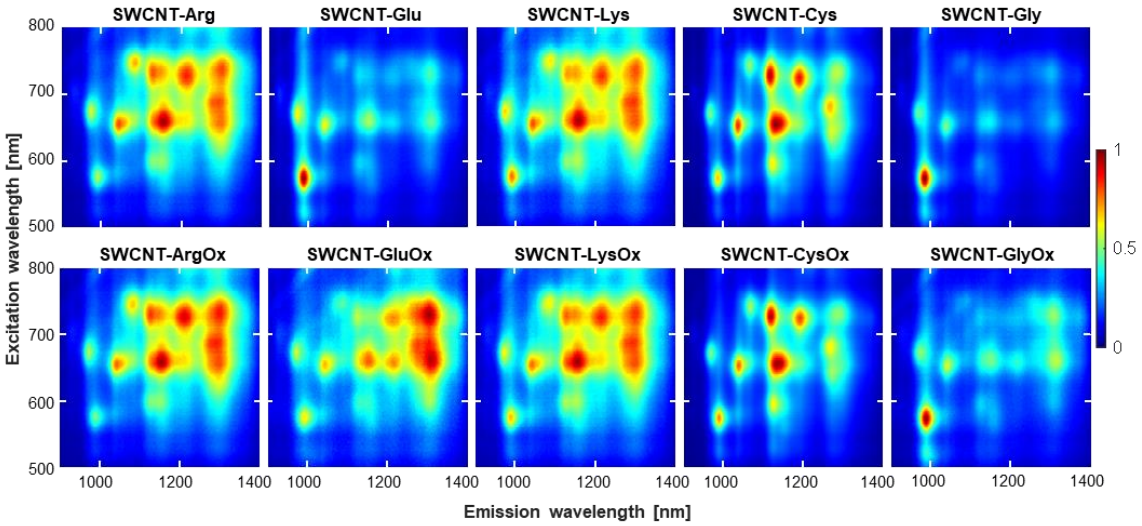

Figure 12. *Excitation emission maps of the SWCNT-peptide suspensions before (top) and after (bottom) oxidation.*

Additional Raman spectroscopy analysis (Figure 13) comparing the spectra of each sensor before and after oxidation revealed no significant changes in the D band peak (around 1350 cm^{-1}), confirming that the sp^2 structure of the nanotubes remained intact. This suggests that the oxidation process was limited to the Fmoc-peptides, leaving the carbon nanotube chemical structure unaltered.

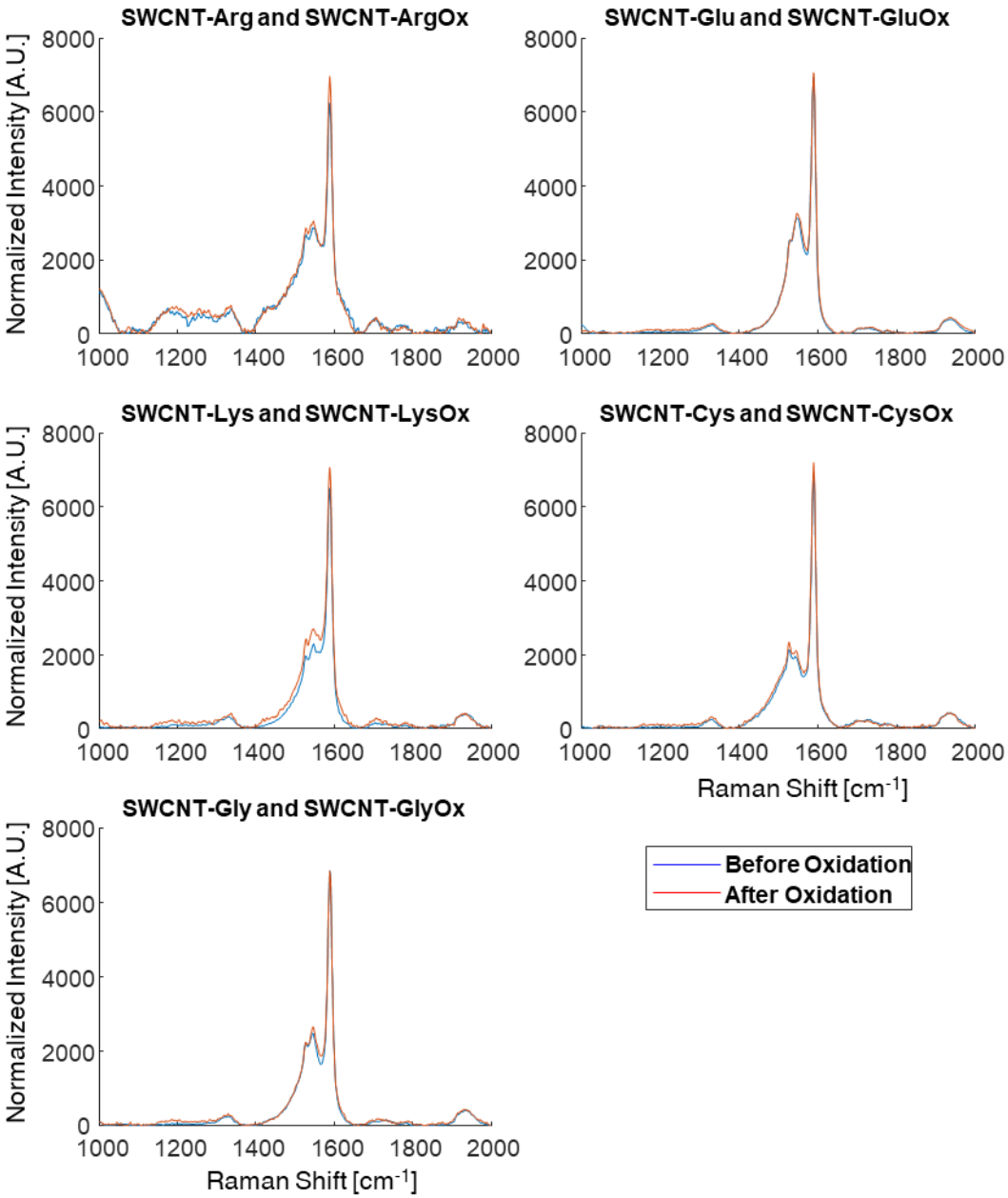

Figure 13. *Raman spectra of the SWCNTs-peptides, before (blue) and after (red) oxidation, showing no significant changes in the D band,* 1350 cm^{-1}, *suggesting conservation of the SWCNT lattice after UV exposure.*

Through the oxidation of the five Fmoc-peptides and the resulting chemically and structurally modified coronae, we obtain ten different SWCNT-peptide sensors. Further, by leveraging the different chiralities present in each SWCNT suspension, specifically focusing on the fluorescence response of three chiralities, (6,5), (7,5), and (9,4), we effectively increase the sensor library to a total of 30 distinct sensors.

3.3 Metal-ion induced sensor fluorescent modulation and fingerprinting.

To establish a fluorescence fingerprinting sensor platform capable of identifying specific analytes from a diverse pool, it is essential to characterize the signal response of each sensor to each analyte. By comprehensively mapping the distinct fluorescence responses of the individual sensors to the various analytes and ensuring sufficient variability in these responses, we can select a subset of the sensors that collectively provide a unique response pattern, or "fingerprint," for each analyte.

To monitor the fluorescence intensity response of each SWCNT-peptide sensor to the transition metal-ions Cu^{2+}, Ni^{2+}, Cr^{3+}, Pb^{2+}, and Hg^{2+}, we subjected each sensor to a metal-ion concentration of 300 μM which was reported to induce measurable changes in fluorescence.[3] For each SWCNT-peptide sensor, we recorded the intensity changes at three different excitation wavelengths, 570 nm, 660 nm, and 730 nm, corresponding to the excitation wavelengths of three chiralities, (6,5), (7,5), and (9,4), respectively. Figure 14a shows the fluorescence emission spectra of one Fmoc-peptide sensor, SWCNT-Glu, excited at 570 nm, with the relative fluorescence response of the corresponding (6,5) chirality to the metal-ions. Notably, the sensor exhibited distinct fluorescence responses to each metal-ion: Ni^{2+}, Cr^{2+}, and Pb^{2+} induced varying degrees of intensity increase, with Ni^{2+} showing the highest increase, while Cu^{2+} and Hg^{2+} caused a decrease in intensity. The nature of the intensity change in response to analyte binding to the SWCNT surface, whether an increase or decrease, remains an area of active research.[47] Nevertheless, as reported in previous works, the fluorescence intensity decrease upon Cu^{2+} and Hg^{2+} might be attributed to fluorescence quenching.[3,111,112]

Achieving a fingerprinting sensor system requires variations in the SWCNT-peptide sensor responses to the different analytes. Indeed, by comparing, for example, the fluorescence response of the (6,5) chirality of three sensors, SWCNT-Glu, SWCNT-GluOx, and SWCNT-Cys, we observed a corona-specific response towards the different metal analytes (Figure 14b). Additionally, the comparison between the responses of SWCNT-Glu and SWCNT-GluOx demonstrates that peptide oxidation leads to variations in fluorescence intensity response to metal addition, confirming the creation of independent sensors via chemical modifications of the peptide corona

through the oxidation process. The relative fluorescence intensity changes of the (6,5) chirality of all ten SWCNT-peptide samples show different response patterns for each metal-ion, thereby generating an analyte-specific fingerprint (Figure 14c).

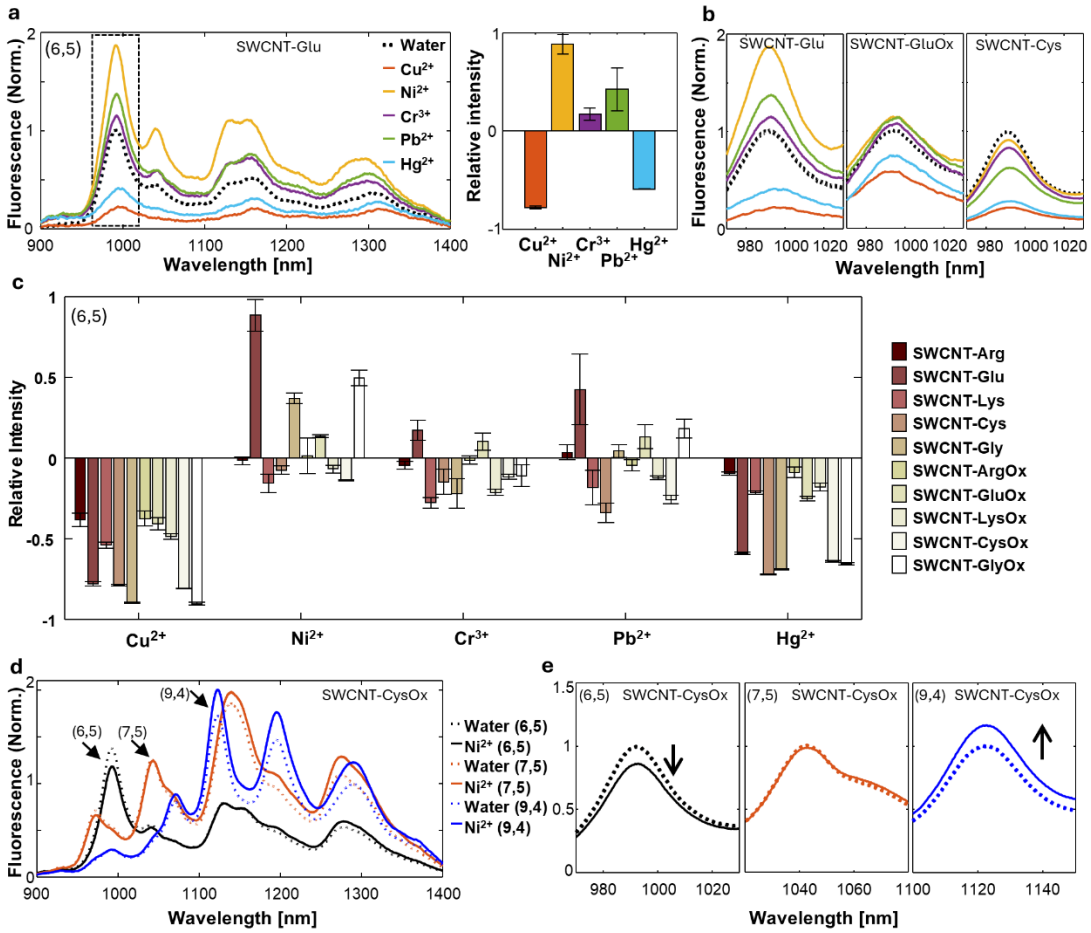

Figure 14. *Fluorescence response of the SWCNT-peptide sensor in the presence of metal-ions. a) Normalized fluorescence emission spectra of SWCNT-Glu, excited at 570 nm, before (dotted black line) and after the addition of metal-ions, Cu^{2+} (orange), Ni^{2+} (yellow), Cr^{3+} (purple), Pb^{2+} (green), and Hg^{2+} (blue). The dashed rectangle marks the peak of (6,5) chirality. The bar plot shows the relative fluorescence response for each metal-ion. N=5 b) Normalized fluorescence intensity of the (6,5) chirality of SWCNT-Glu, SWCNT-GluOx, and SWCNT-Cys before (dotted black line) and after the addition of metals-ions, Cu^{2+} (orange), Ni^{2+} (yellow), Cr^{3+} (purple), Pb^{2+} (green), and Hg^{2+} (blue). c) Bar plot of the relative fluorescence response of the (6,5) chirality of all the SWCNT-peptide sensors in the presence of the metal-ions. N=5 d) Normalized fluorescence emission spectra of SWCNT-CysOx in water (dotted lines) and after the addition of Ni^{2+} (continuous lines), measured at three excitation wavelengths: 570 nm (black), 660 nm (orange), and 730 nm (blue), corresponding to the excitation wavelengths of the (6,5), (7,5), and (9,4) chiralities, respectively. Arrows mark the peaks of the respective*

chiralities. e) Normalized fluorescence intensity of the (6,5), (7,5), and (9,4) chirality of SWCNT-CysOx before (dotted lines) and after the addition of Ni^{2+} (continuous lines).

HiPCO SWCNT samples contain a mixture of different chiralities within a single suspension, where the differences in their optical properties enable us to treat each chirality as a single sensor probed by its distinct excitation and emission wavelengths.[45,93,95,96,113–116] The fluorescence response of SWCNT-CysOx in the presence of Ni^{2+} measured at three different excitation wavelengths corresponding to the three chiralities (6,5), (7,5), and (9,4), exemplifies this point (Figure 14d), showing a turn-off response of the (6,5) chirality, no significant change of the (7,5) chirality, and a turn-on response for the (9,4) chirality (Figure 14e). These results demonstrate that each chirality of a SWCNT-peptide sample can have a distinct response to a particular analyte and, thus, can be regarded as an independent sensor. Figure 15 shows the bar plots for the relative fluorescence intensity changes of all the SWCNT-peptide sensors when interacting with the metal-ions for all three chiralities.

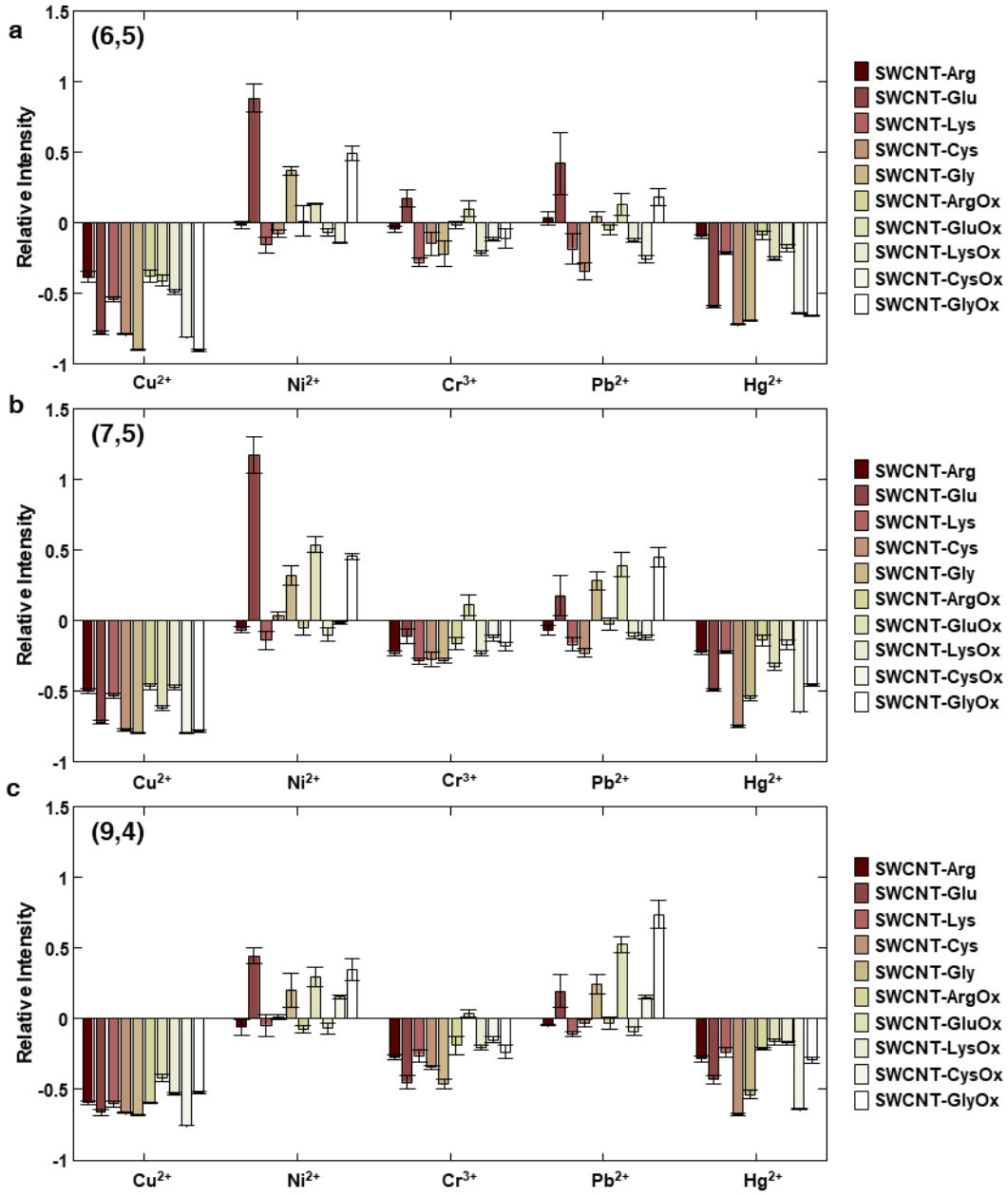

Figure 15. *Relative fluorescence response of the SWCNT-peptide sensors to each metal for three different chiralities, a) (6,5), b) (7,5), and c) (9,4), excited at 570 nm, 660 nm, and 730 nm, respectively. N=5.*

In our sensing model, it is reasonable to expect that the variations in the fluorescence responses of the SWCNT-peptide sensors toward the analytes are due to the different binding affinities of metal-ions to the functional groups offered by the peptide-coronae or different wrapping conformations adopted by the corona phases. We observe that the sensor response is not clearly correlated with the Fmoc-peptide coverage per SWCNTs, suggesting that a higher peptide loading does not automatically result in a higher

fluorescence response to metal-ions (Figure 16a). Furthermore, the zeta potential of the SWCNT-peptide sensors does not show a clear correlation with metal adsorption either (Figure 16b). Specifically, a negative zeta potential does not consistently lead to a higher fluorescence response by adsorbing more positively charged metal-ions. These findings suggest that the peptide structure variations, indeed, contribute to the fluorescence responses of the SWCNT-peptide sensors to the metal-ions.

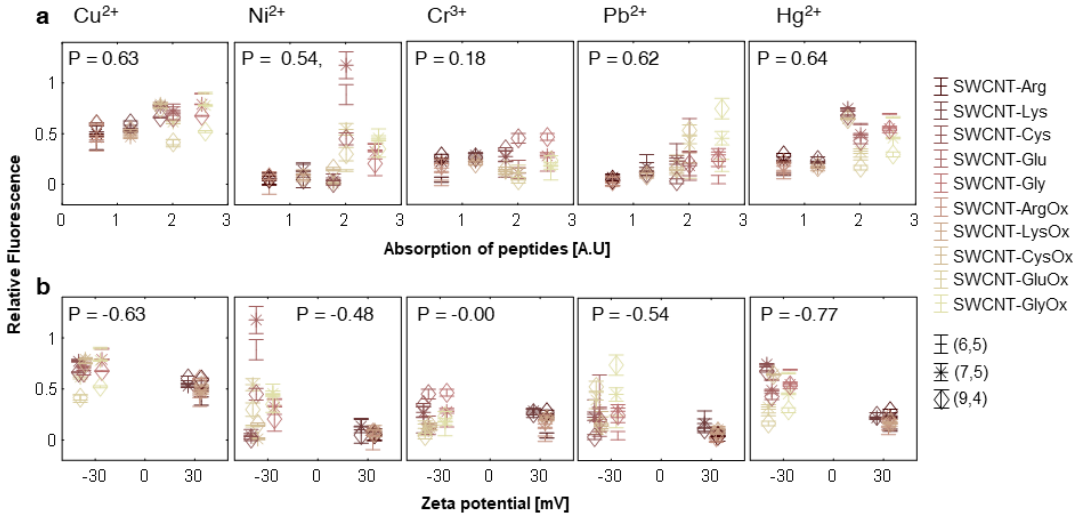

Figure 16. *Correlation of the absolute relative fluorescence response of the SWCNT-peptide sensors to the peptide surface coverage or the zeta potential. a) Absolute relative fluorescence change and the Pearson correlation coefficient, P, of the thirty sensors upon adding metal-ions vs. the absorption of the Fmoc-group at 270 nm in the suspension, indicative of the peptide load on the SWCNT surface. N=3 b) Absolute relative fluorescence change and the Pearson correlation coefficient, P, of the 30 SWCNT-peptide sensors upon adding metal-ions vs. the zeta potential of the SWCNTs. N=3.*

3.4 Sensor set optimization.

To create a cost and time-efficient sensor platform, minimizing the number of sensors needed to identify a specific analyte is beneficial. For example, identifying Ni^{2+} does not require all 30 sensors, but rather, a subset of a small number of sensors can be sufficient to achieve a distinctive fingerprint. As an example, a turn-on response of the (9,4) chirality of SWCNT-GlyOx suggests the presence of either Ni^{2+} or Pb^{2+}, as the other metal-ions would induce a decrease in the fluorescence intensity (Figure 17a). A subsequent experiment with the (7,5) chirality of SWCNT-Cys showing a small turn-on response in the fluorescence intensity would point towards Ni^{2+} since Pb^{2+} would have induced a fluorescence intensity decrease (Figure 17b). An additional experiment with the (7,5) chirality of SWCNT-Glu showing a significant turn-on response would confirm the presence of Ni^{2+} rather than Pb^{2+}, as the latter would have caused only a slight increase in the emission intensity (Figure 17c). Therefore, to identify Ni^{2+} out of the five metal-ions, only two or three sensors would be sufficient. In our example, two sensors, SWCNT-GlyOx-(9,4) and SWCNT-Cys-(7,5), can identify the analyte, and a third sensor, SWCNT-Glu-(7,5), would simply increase the certainty of the sensing experiment.

Complete sensor set optimization was performed by the ACFSA algorithm by Michael Faran, which indicated that two sensors, SWCNT-Gly-(6,5) and SWCNT-GlyOx-(6,5), are enough to classify the metals with an error of less than 0.02%

Future work would involve increasing the dataset by exploiting multiple variables, such as concentrations, analyte mixtures, environments, and additional chiralities.

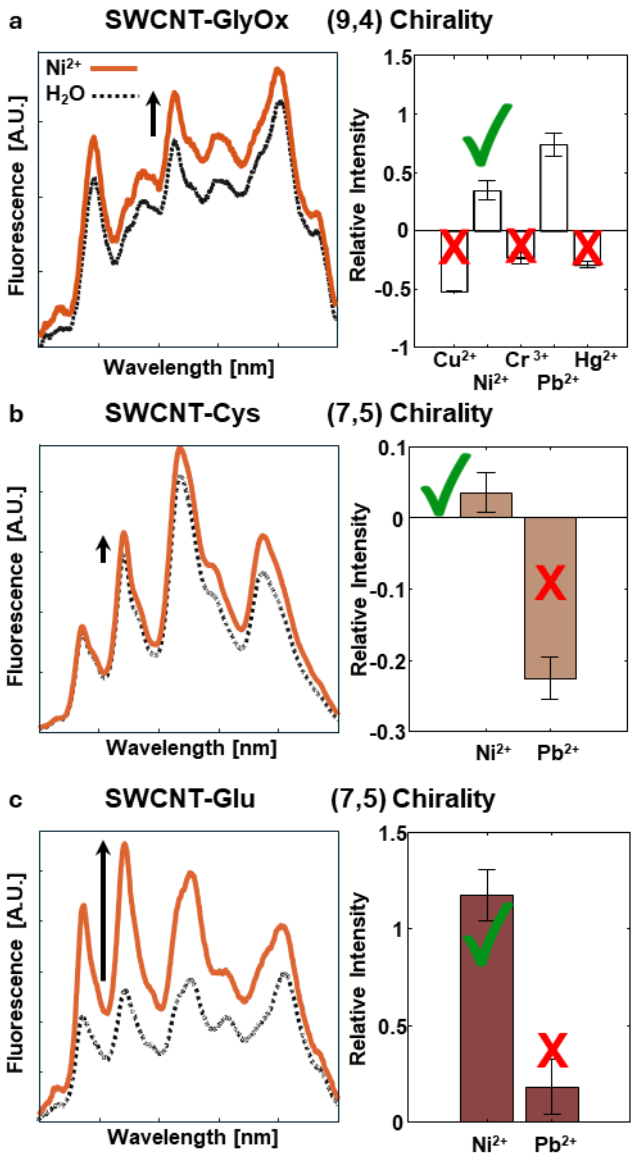

Figure 17. *Example of an analyte identification procedure using several sensors. a) The (9,4) chirality of SWCNT-GlyOx shows an intensity increase in response to the analyte, indicating* Ni^{2+} *or* Pb^{2+}*. b) A turn-on response of the (7,5) chirality of SWCNT-Cys excludes* Pb^{2+}*. c) Significant turn-on response of the (7,5) chirality of SWCNT-Glu further confirms* Ni^{2+}*, in contrast to a minor turn-on response that would indicate* Pb^{2+}*. N=5.*

3.5 Limit of detection, functionality in mineral water and serum

To further explore the response of sensors to different concentrations and identify detection limits, we performed an analysis on SWCNT-Gly-(6,5), the sensor selected by Michael Faran's ACFSA algorithm as the most variable in the fluorescent signals it provided for all the analytes for identification purposes. The concentration-dependent responses for all tested metal ions are shown in Figure 18, revealing detection limits of $3.0x10^{-9}$ M for copper, $7.2x10^{-5}$ M for chrome, $7.1x10^{-7}$ M for mercury, $8.1x10^{-6}$ M for lead, and $3.6x10^{-5}$ M for nickel. While these results indicate variability in detection limits for the identification of analytes, it is important to note that this analysis does not imply SWCNT-Gly is the most sensitive sensor for a specific analyte but rather demonstrates its utility for identification tasks across varying concentrations. Importantly, these findings show that fingerprint patterns, meaning the absolute increase or decrease in fluorescence, are preserved for certain analytes even when concentration varies, highlighting the potential to extend this approach to larger datasets spanning a broader range of concentrations for analyte identification and sensor selection.

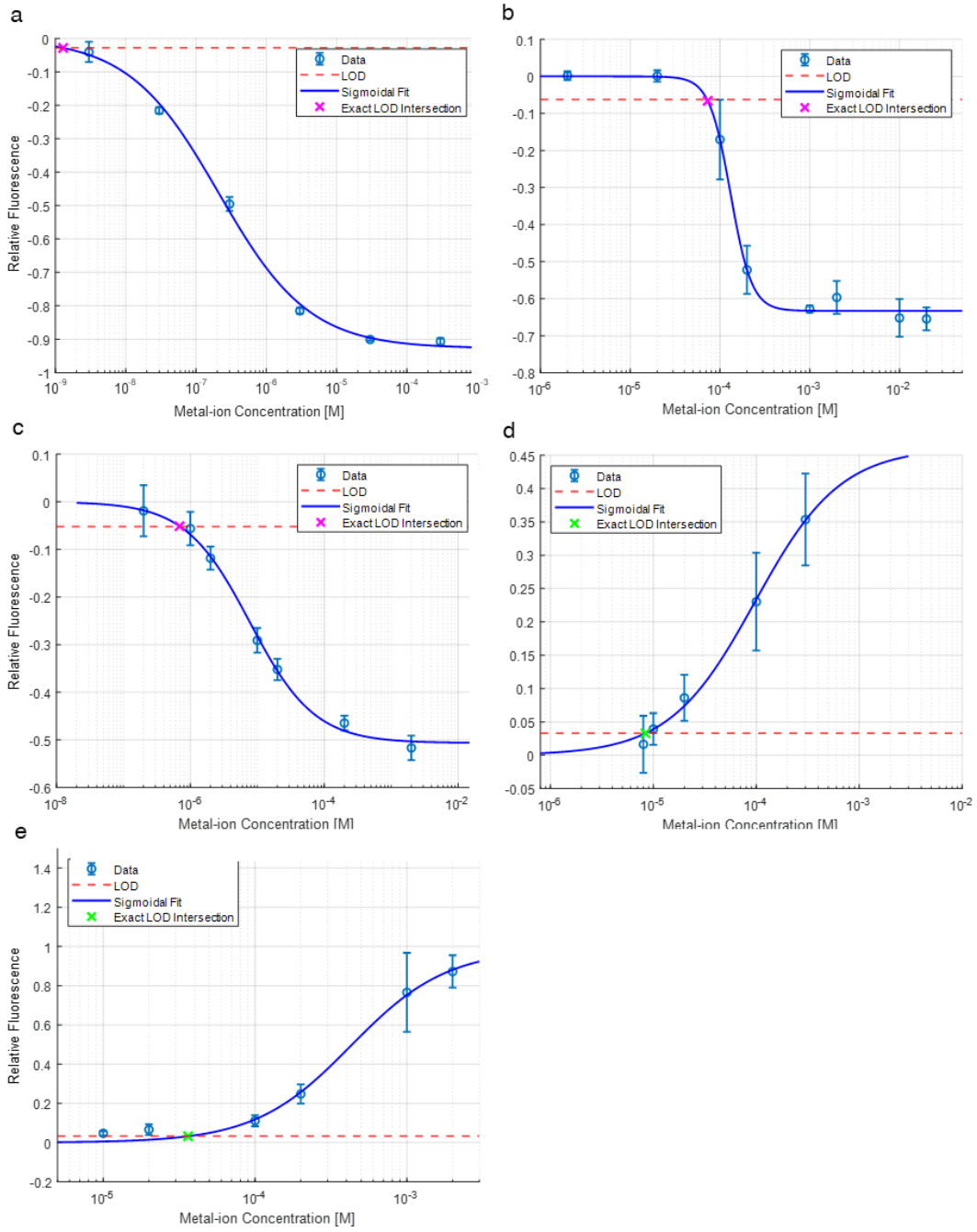

Figure 18. *Relative fluorescent response of the sensor SWCNT-Gly vs. different metal-ion concentrations measured in triplicates. Data points with error bars and sigmoidal fit of the data (blue), 3 times the STD value of the sensor alone (dashed red) and, intersection marked with a green X. Limit of detection for a) Copper: 3.0x10^{-9} M, b) Chrome: 7.2x10^{-5} M, c) Mercury: 7.1x10^{-7} M, d) Lead: 8.1x10^{-6} M, and e) Nickel: 3.6x10^{-5} M. N=3.*

To further assess the potential functionality of these sensors in different environments, additional experiments measuring the response of the SWCNT-Gly

sensor to the analytes were conducted in fetal bovine serum and in commercial mineral water (Figure 19). Both environments produced distinct fingerprinting patterns, although they differed from those observed in water, probably due to the interaction of both the SWCNTs-peptides and the metal-ions with other serum components or, with the dissolved minerals or other anions in mineral water. These results suggest that SWCNT-Gly, and potentially other sensors as well, could generate fingerprinting capabilities across diverse matrices. However, variations in the content and pH of each environment may necessitate adjustments to the peptide library and require the generation of new fingerprinting datasets to account for these matrix-specific factors.

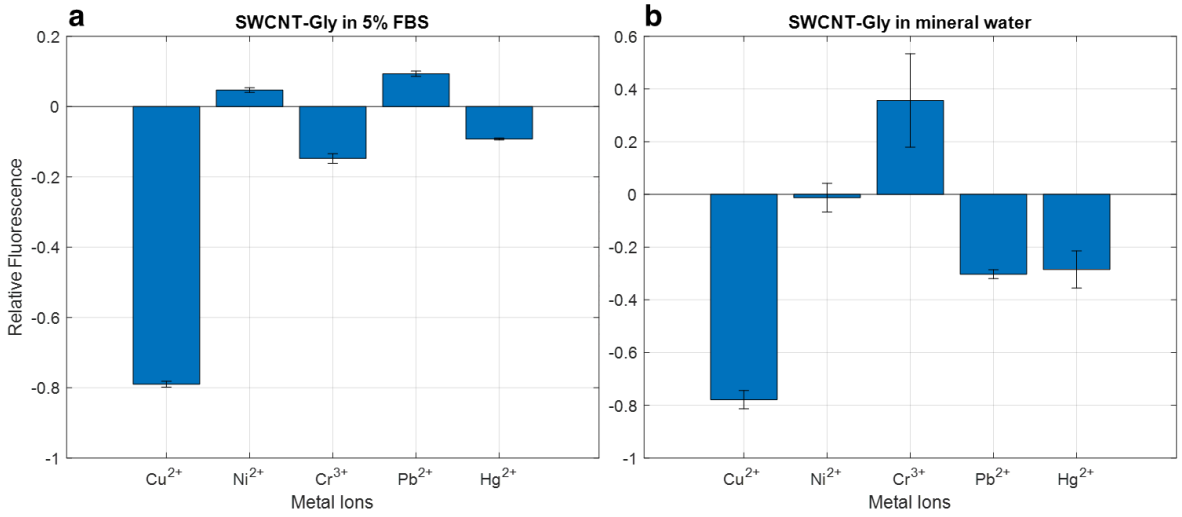

Figure 19. *Relative fluorescence response of the sensor SWCNT-Gly to five metal-ions, Cu2+, Ni2+, Cr3+, Pb2+, and Hg2+, in a) fetal bovine serum and b) commercial mineral water. N=5.*

These analyses highlight the adaptability of the peptide-SWCNT sensor system and extend its potential application for analyte identification and sensor selection to a broader range of environmental and biological conditions.

4. Conclusion

We present a comprehensive approach to synthesize Fmoc-peptide functionalized SWCNTs with varying amino acids in the peptide sequence, as the corona phase, to generate a near-infrared fluorescent sensor library for transition metal-ion fingerprinting and identification. We showed that the Fmoc-peptides we designed can form stable SWCNT suspensions in water while maintaining the NIR fluorescence of the SWCNTs. Further, the peptides underwent photochemical dimerization and oxidation of the tyrosine side chains when exposed to UV light, inducing structural and chemical changes in the peptide corona, which, along with the three analyzed chiralities, (6,5), (7,5), and (9,4), in the SWCNT-peptide samples, extended the SWCNT-peptide sensor library to 30 sensors.

Exposing the SWCNT-peptide sensors to transition metal-ions such as Cu^{2+}, Ni^{2+}, Cr^{3+}, Pb^{2+}, and Hg^{2+}, and measuring their fluorescence intensity modulations for each chirality, revealed a distinct fluorescence response pattern for each SWCNT-peptide sensor to the different metal-ions, rendering them suitable for constructing a fingerprint library for the identification of the five analytes.

Additionally, we demonstrated that the selected test sensor, SWCNT-Gly-(6,5), maintained the absolute fingerprint patterns even with concentration variation, with limits of detection varying from the nanomolar range for copper to the micromolar range for nickel. These results underscore the potential for extending this approach to more comprehensive datasets that include a wide range of analyte concentrations for every sensor. Future work should focus on extending the fingerprinting power by testing responses in multiple working concentrations, mixtures of analytes and environments, in vitro or in vivo, to fully harness the identification capabilities of this approach.

The methodology developed here can be generalized and applied to synthesize other corona phase sensors and perform analyte screening experiments. The variability of peptide sequences, natural and artificial, as well as any secondary modifications, oxidations, or peptide chain chemical alterations, generates an enormous pool of sensor possibilities.

This, coupled with the optical and physicochemical properties of the single-walled carbon nanotubes, and the new possibilities for covalent functionalizations, paves the

way for future advancements in fingerprinting sensor technology and its application to identify diverse molecular analytes.

5. References

(1) Morales, M. A.; Halpern, J. M. Guide to Selecting a Biorecognition Element for Biosensors. *Bioconjug. Chem.* **2018**, *29*, 3231–3239.

(2) Kim, D. C.; Kang, D. J. Molecular Recognition and Specific Interactions for Biosensing Applications. *Sensors* **2008**, *8*, 6605–6641.

(3) Wulf, V.; Bichachi, E.; Hendler-Neumark, A.; Massarano, T.; Leshem, A. B.; Lampel, A.; Bisker, G.; Hendler-Neumark, A.; Massarano, T.; Leshem, A. B.; Lampel, A.; Bisker, G. Multicomponent System of Single-Walled Carbon Nanotubes Functionalized with a Melanin-Inspired Material for Optical Detection and Scavenging of Metals. *Adv. Funct. Mater.* **2022**, *32*, 2209688.

(4) Blake, D. A.; Jones, R. M.; Blake, R. C.; Pavlov, A. R.; Darwish, I. A.; Yu, H. Antibody-Based Sensors for Heavy Metal Ions. *Biosens. Bioelectron.* **2001**, *16*, 799–809.

(5) Carter, K. P.; Young, A. M.; Palmer, A. E. Fluorescent Sensors for Measuring Metal Ions in Living Systems. *Chem. Rev.* **2014**, *114*, 4564–4601.

(6) El-Safty, S. A.; Prabhakaran, D.; Ismail, A. A.; Matsunaga, H.; Mizukami, F. Nanosensor Design Packages: A Smart and Compact Development for Metal Ions Sensing Responses. *Adv. Funct. Mater.* **2007**, *17*, 3731–3745.

(7) Zhang, L.; Peng, D.; Liang, R.-P.; Qiu, J.-D. Graphene-Based Optical Nanosensors for Detection of Heavy Metal Ions. *TrAC Trends Anal. Chem.* **2018**, *102*, 280–289.

(8) Cho, E. J.; Lee, J.-W.; Ellington, A. D. Applications of Aptamers as Sensors. *Annu. Rev. Anal. Chem.* **2009**, *2*, 241–264.

(9) Byrne, B.; Stack, E.; Gilmartin, N.; O'Kennedy, R. Antibody-Based Sensors: Principles, Problems and Potential for Detection of Pathogens and Associated Toxins. *Sensors* **2009**, *9*, 4407–4445.

(10) Nguyen, H. H.; Lee, S. H.; Lee, U. J.; Fermin, C. D.; Kim, M. Immobilized Enzymes in Biosensor Applications. *Materials (Basel).* **2019**, *12*, 121.

(11) Zhang, J.; Landry, M. P.; Barone, P. W.; Kim, J.-H.; Lin, S.; Ulissi, Z. W.; Lin, D.; Mu, B.; Boghossian, A. A.; Hilmer, A. J.; Rwei, A.; Hinckley, A. C.; Kruss, S.; Shandell, M. A.; Nair, N.; Blake, S.; Şen, F.; Şen, S.; Croy, R. G.; Li, D.; Yum, K.; Ahn, J.-H.; Jin, H.; Heller, D. A.; Essigmann, J. M.; Blankschtein, D.; Strano, M. S. Molecular Recognition Using Corona Phase Complexes Made of Synthetic Polymers Adsorbed on Carbon Nanotubes. *Nat. Nanotechnol.* **2013**, *8*, 959–968.

(12) Bisker, G.; Dong, J.; Park, H. D.; Iverson, N. M.; Ahn, J.; Nelson, J. T.; Landry, M. P.; Kruss, S.; Strano, M. S. Protein-Targeted Corona Phase Molecular Recognition. *Nat. Commun.* **2016**, *7*, 10241.

(13) Yotova, L.; Yaneva, S.; Marinkova, D. Biomimetic Nanosensors for Determination of Toxic Compounds in Food and Agricultural Products (Review). *J. Univ. Chem. Technol. Metall.* **2013**, *48*, 215–227.

(14) Denizli, A. Molecular Imprinting for Nanosensors and Other Sensing Applications. *Mol. Imprinting Nanosensors Other Sens. Appl.* **2021**, 1–417.

(15) Adampourezare, M.; Nikzad, B.; Nasrollahzadeh, S.; Asadpour-Zeynali, K.; de la Guardia, M.; Ezzati Nazhad Dolatabadi, J.; Zhang, F.; Mahdi Jafari, S. Polysaccharide-Based Sensors and Nanosensors: A Review of Recent Progress and Challenges. *Microchem. J.* **2024**, *204*, 110944.

(16) Nocerino, V.; Miranda, B.; Tramontano, C.; Chianese, G.; Dardano, P.; Rea, I.; De Stefano, L. Plasmonic Nanosensors: Design, Fabrication, and Applications in Biomedicine. *Chemosensors* **2022**, *10*, 150.

(17) Zhang, L.; Yang, Y.; Tan, J.; Yuan, Q. Chemically Modified Nucleic Acid Biopolymers Used in Biosensing. *Mater. Chem. Front.* **2020**, *4*, 1315–1327.

(18) Shumeiko, V.; Zaken, Y.; Hidas, G.; Paltiel, Y.; Bisker, G.; Shoseyov, O. Peptide-Encapsulated Single-Wall Carbon Nanotube-Based Near-Infrared Optical Nose for Bacteria Detection and Classification. *IEEE Sens. J.* **2022**, *22*, 6277–6287.

(19) Zong, C.; Fang, L.; Song, F.; Wang, A.; Wan, Y. Fluorescent Fingerprint Bacteria by Multi-Channel Magnetic Fluorescent Nanosensor. *Sensors Actuators B Chem.* **2019**, *289*, 234–241.

(20) Amir, D.; Hendler-Neumark, A.; Wulf, V.; Ehrlich, R.; Bisker, G. Oncometabolite Fingerprinting Using Fluorescent Single-Walled Carbon Nanotubes. *Adv. Mater. Interfaces* **2022**, *9*.

(21) Kim, M.; Chen, C.; Wang, P.; Mulvey, J. J.; Yang, Y.; Wun, C.; Antman-Passig, M.; Luo, H.-B.; Cho, S.; Long-Roche, K.; Ramanathan, L. V.; Jagota, A.; Zheng, M.; Wang, Y.; Heller, D. A. Detection of Ovarian Cancer via the Spectral Fingerprinting of Quantum-Defect-Modified Carbon Nanotubes in Serum by Machine Learning. *Nat. Biomed. Eng.* **2022**, *6*, 267–275.

(22) Nißler, R.; Bader, O.; Dohmen, M.; Walter, S. G.; Noll, C.; Selvaggio, G.; Groß, U.; Kruss, S. Remote near Infrared Identification of Pathogens with Multiplexed Nanosensors. *Nat. Commun.* **2020**, *11*, 5995.

(23) Ebrahim-Habibi, M.-B.; Ghobeh, M.; Mahyari, F. A.; Rafii-Tabar, H.; Sasanpour, P. An Investigation into Non-Covalent Functionalization of a Single-Walled Carbon Nanotube and a Graphene Sheet with Protein G:A Combined Experimental and Molecular Dynamics Study. *Sci. Rep.* **2019**, *9*, 1273.

(24) Sultana, N.; Dewey, H. M.; Arellano, A. G.; Budhathoki-Uprety, J. Understanding the Molecular Assemblies of Single Walled Carbon Nanotubes and Tailoring Their Photoluminescence for the Next-Generation Optical Nanosensors. *Chem. Mater.* **2024**, *36*, 4034–4053.

(25) Ramezani, F.; Rafii-Tabar, H. An In-Depth View of Human Serum Albumin Corona on Gold Nanoparticles. *Mol. Biosyst.* **2015**, *11*, 454–462.

(26) Zuo, G.; Zhou, X.; Huang, Q.; Fang, H.; Zhou, R. Adsorption of Villin Headpiece onto Graphene, Carbon Nanotube, and C60: Effect of Contacting Surface Curvatures on Binding Affinity. *J. Phys. Chem. C* **2011**, *115*, 23323–

23328.

(27) Harrison, E. T.; Weidner, T.; Castner, D. G.; Interlandi, G. Predicting the Orientation of Protein G B1 on Hydrophobic Surfaces Using Monte Carlo Simulations. *Biointerphases* **2017**, *12*.

(28) Xiao, H.; Huang, B.; Yao, G.; Kang, W.; Gong, S.; Pan, H.; Cao, Y.; Wang, J.; Zhang, J.; Wang, W. Atomistic Simulation of the Coupled Adsorption and Unfolding of Protein GB1 on the Polystyrenes Nanoparticle Surface. *Sci. China Physics, Mech. Astron.* **2018**, *61*, 038711.

(29) Lambert, B. P.; Taheri, A.; Wu, S.-J.; Gillen, A. J.; Kashaninejad, M.; Boghossian, A. A. Directed Evolution of Nanosensors for the Detection of Mycotoxins. *bioRxiv*. June 14, 2023.

(30) An, S.; Suh, Y.; Kelich, P.; Lee, D.; Vukovic, L.; Jeong, S. Directed Evolution of Near-Infrared Serotonin Nanosensors with Machine Learning-Based Screening. *Nanomaterials* **2024**, *14*, 247.

(31) Jeong, S.; Yang, D.; Beyene, A. G. G.; Del Bonis-O'Donnell, J. T. T.; Gest, A. M. M. M.; Navarro, N.; Sun, X.; Landry, M. P. P. High-Throughput Evolution of near-Infrared Serotonin Nanosensors. *Sci. Adv.* **2019**, *5*, eaay3771.

(32) Conroy, P. J.; Hearty, S.; Leonard, P.; O'Kennedy, R. J. Antibody Production, Design and Use for Biosensor-Based Applications. *Semin. Cell Dev. Biol.* **2009**, *20*, 10–26.

(33) Bettinger, H. F. Carbon Nanotubes—Basic Concepts and Physical Properties. By S. Reich, C. Thomsen, J. Maultzsch. *ChemPhysChem* **2004**, *5*, 1914–1915.

(34) Kruss, S.; Hilmer, A. J.; Zhang, J.; Reuel, N. F.; Mu, B.; Strano, M. S. Carbon Nanotubes as Optical Biomedical Sensors. *Adv. Drug Deliv. Rev.* **2013**, *65*, 1933–1950.

(35) Bachilo, S. M.; Strano, M. S.; Kittrell, C.; Hauge, R. H.; Smalley, R. E.; Weisman, R. B. Structure-Assigned Optical Spectra of Single-Walled Carbon Nanotubes. *Science* **2002**, *298*, 2361–2366.

(36) Ackermann, J.; Metternich, J. T.; Herbertz, S.; Kruss, S. Biosensing with Fluorescent Carbon Nanotubes. *Angew. Chemie Int. Ed.* **2022**, *61*, e202112372.

(37) Weisman, R. B.; Bachilo, S. M. Dependence of Optical Transition Energies on Structure for Single-Walled Carbon Nanotubes in Aqueous Suspension: An Empirical Kataura Plot. *Nano Lett.* **2003**, *3*, 1235–1238.

(38) Qiu, L.; Ding, F. Understanding Single-Walled Carbon Nanotube Growth for Chirality Controllable Synthesis. *Accounts Mater. Res.* **2021**, *2*, 828–841.

(39) Irita, M.; Yamamoto, T.; Homma, Y. Chirality Distributions for Semiconducting Single-Walled Carbon Nanotubes Determined by Photoluminescence Spectroscopy. *Nanomaterials* **2021**, *11*, 2309.

(40) Bonis-O'Donnell, J. T. Del; Page, R. H.; Beyene, A. G.; Tindall, E. G.; McFarlane, I. R.; Landry, M. P. Dual Near-Infrared Two-Photon Microscopy for Deep-Tissue Dopamine Nanosensor Imaging. *Adv. Funct. Mater.* **2017**, *27*.

(41) Iverson, N. M.; Barone, P. W.; Shandell, M.; Trudel, L. J.; Sen, S.; Sen, F.; Ivanov, V.; Atolia, E.; Farias, E.; McNicholas, T. P.; Reuel, N.; Parry, N. M. A.; Wogan, G. N.; Strano, M. S. In Vivo Biosensing via Tissue-Localizable near-Infrared-Fluorescent Single-Walled Carbon Nanotubes. *Nat. Nanotechnol.* **2013**, *8*, 873–880.

(42) Hendler-Neumark, A.; Wulf, V.; Bisker, G. In Vivo Imaging of Fluorescent Single-Walled Carbon Nanotubes within C. Elegans Nematodes in the near-Infrared Window. *Mater. Today Bio* **2021**, *12*, 100175.

(43) Iverson, N. M.; Bisker, G.; Farias, E.; Ivanov, V.; Ahn, J.; Wogan, G. N.; Strano, M. S. Quantitative Tissue Spectroscopy of Near Infrared Fluorescent Nanosensor Implants. *J. Biomed. Nanotechnol.* **2016**, *12*, 1035–1047.

(44) Nandi, S.; Caicedo, K.; Cognet, L. When Super-Resolution Localization Microscopy Meets Carbon Nanotubes. *Nanomaterials* **2022**, *12*, 1433.

(45) Barone, P. W.; Baik, S.; Heller, D. A.; Strano, M. S. Near-Infrared Optical Sensors Based on Single-Walled Carbon Nanotubes. *Nat. Mater.* **2005**, *4*, 86–92.

(46) Boghossian, A. A.; Zhang, J.; Barone, P. W.; Reuel, N. F.; Kim, J.; Heller, D. A.; Ahn, J.; Hilmer, A. J.; Rwei, A.; Arkalgud, J. R.; Zhang, C. T.; Strano, M. S. Near-Infrared Fluorescent Sensors Based on Single-Walled Carbon Nanotubes for Life Sciences Applications. *ChemSusChem* **2011**, *4*, 848–863.

(47) Nißler, R.; Ackermann, J.; Ma, C.; Kruss, S. Prospects of Fluorescent Single-Chirality Carbon Nanotube-Based Biosensors. *Anal. Chem.* **2022**, *94*, 9941–9951.

(48) Zhang, Y.; Guo, J.; Tang, Z.; Tang, C.; Li, Y.; Tao, X.; Zhou, B.; Chen, W.; Guo, L.; Tang, K.; Liang, T. Recent Developments and Trends of Biosensors Based on Carbon Nanotubes for Biomedical Diagnosis Applications: A Review. *Biosens. Bioelectron. X* **2024**, *17*, 100424.

(49) Murjani, B. O.; Kadu, P. S.; Bansod, M.; Vaidya, S. S.; Yadav, M. D. Carbon Nanotubes in Biomedical Applications: Current Status, Promises, and Challenges. *Carbon Lett.* **2022**, *32*, 1207–1226.

(50) Acharya, R.; Patil, T. V.; Dutta, S. D.; Lee, J.; Ganguly, K.; Kim, H.; Randhawa, A.; Lim, K. Single-Walled Carbon Nanotube-Based Optical Nano/Biosensors for Biomedical Applications: Role in Bioimaging, Disease Diagnosis, and Biomarkers Detection. *Adv. Mater. Technol.* **2024**, 2400279.

(51) Yaari, Z.; Cheung, J. M.; Baker, H. A.; Frederiksen, R. S.; Jena, P. V.; Horoszko, C. P.; Jiao, F.; Scheuring, S.; Luo, M.; Heller, D. A. Nanoreporter of an Enzymatic Suicide Inactivation Pathway. *Nano Lett.* **2020**, *20*, 7819–7827.

(52) Kallmyer, N. E.; Abdennadher, M. S.; Agarwal, S.; Baldwin-Kordick, R.; Khor, R. L.; Kooistra, A. S.; Peterson, E.; McDaniel, M. D.; Reuel, N. F. Inexpensive Near-Infrared Fluorimeters: Enabling Translation of NIR-Based Assays to the Field. *Anal. Chem.* **2021**, *93*, 4800–4808.

(53) Dong, J.; Lee, M. A. A.; Rajan, A. G. G.; Rahaman, I.; Sun, J. H. H.; Park, M.; Salem, D. P. P.; Strano, M. S. S. A Synthetic Mimic of Phosphodiesterase Type

5 Based on Corona Phase Molecular Recognition of Single-Walled Carbon Nanotubes. *Proc. Natl. Acad. Sci.* **2020**, *117*.

(54) Wulf, V.; Slor, G.; Rathee, P.; Amir, R. J.; Bisker, G. Dendron–Polymer Hybrids as Tailorable Responsive Coronae of Single-Walled Carbon Nanotubes. *ACS Nano* **2021**, *15*, 20539–20549.

(55) Basu, S.; Hendler-Neumark, A.; Bisker, G. Rationally Designed Functionalization of Single-Walled Carbon Nanotubes for Real-Time Monitoring of Cholinesterase Activity and Inhibition in Plasma. *Small* **2024**, *20*.

(56) Basu, S.; Hendler-Neumark, A.; Bisker, G. Monitoring Enzyme Activity Using Near-Infrared Fluorescent Single-Walled Carbon Nanotubes. *ACS Sensors* **2024**, *9*, 2237–2253.

(57) Williams, R. M.; Harvey, J. D.; Budhathoki-Uprety, J.; Heller, D. A. Glutathione-S-Transferase Fusion Protein Nanosensor. *Nano Lett.* **2020**, *20*, 7287–7295.

(58) Ehrlich, R.; Hendler-Neumark, A.; Wulf, V.; Amir, D.; Bisker, G. Optical Nanosensors for Real-Time Feedback on Insulin Secretion by B-Cells. *Small* **2021**, *17*, 2101660.

(59) Pinals, R. L.; Ledesma, F.; Yang, D.; Navarro, N.; Jeong, S.; Pak, J. E.; Kuo, L.; Chuang, Y.-C.; Cheng, Y.-W.; Sun, H.-Y.; Landry, M. P. Rapid SARS-CoV-2 Spike Protein Detection by Carbon Nanotube-Based Near-Infrared Nanosensors. *Nano Lett.* **2021**, *21*, 2272–2280.

(60) Nelson, J. T.; Kim, S.; Reuel, N. F.; Salem, D. P.; Bisker, G.; Landry, M. P.; Kruss, S.; Barone, P. W.; Kwak, S.; Strano, M. S. Mechanism of Immobilized Protein A Binding to Immunoglobulin G on Nanosensor Array Surfaces. *Anal. Chem.* **2015**, *87*, 8186–8193.

(61) Gillen, A. J.; Siefman, D. J.; Wu, S.-J.; Bourmaud, C.; Lambert, B.; Boghossian, A. A. Templating Colloidal Sieves for Tuning Nanotube Surface Interactions and Optical Sensor Responses. *J. Colloid Interface Sci.* **2020**, *565*, 55–62.

(62) Kruss, S.; Landry, M. P.; Vander Ende, E.; Lima, B. M. A.; Reuel, N. F.; Zhang, J.; Nelson, J.; Mu, B.; Hilmer, A.; Strano, M. Neurotransmitter Detection Using Corona Phase Molecular Recognition on Fluorescent Single-Walled Carbon Nanotube Sensors. *J. Am. Chem. Soc.* **2014**, *136*, 713–724.

(63) Beyene, A. G. G.; Delevich, K.; Del Bonis-O'Donnell, J. T. T.; Piekarski, D. J. J.; Lin, W. C. C.; Thomas, A. W. W.; Yang, S. J. J.; Kosillo, P.; Yang, D.; Prounis, G. S. S.; Wilbrecht, L.; Landry, M. P. P. Imaging Striatal Dopamine Release Using a Nongenetically Encoded near Infrared Fluorescent Catecholamine Nanosensor. *Sci. Adv.* **2019**, *5*, eaaw3108.

(64) Dinarvand, M.; Elizarova, S.; Daniel, J.; Kruss, S. Imaging of Monoamine Neurotransmitters with Fluorescent Nanoscale Sensors. *Chempluschem* **2020**, *85*, 1465–1480.

(65) Lee, M. A.; Wang, S.; Jin, X.; Bakh, N. A.; Nguyen, F. T.; Dong, J.; Silmore,

K. S.; Gong, X.; Pham, C.; Jones, K. K.; Muthupalani, S.; Bisker, G.; Son, M.; Strano, M. S. Implantable Nanosensors for Human Steroid Hormone Sensing In Vivo Using a Self-Templating Corona Phase Molecular Recognition. *Adv. Healthc. Mater.* **2020**, *9*.

(66) Wong, M. H.; Giraldo, J. P.; Kwak, S.-Y.; Koman, V. B.; Sinclair, R.; Lew, T. T. S.; Bisker, G.; Liu, P.; Strano, M. S. Nitroaromatic Detection and Infrared Communication from Wild-Type Plants Using Plant Nanobionics. *Nat. Mater.* **2017**, *16*, 264–272.

(67) Safaee, M. M. M.; Gravely, M.; Roxbury, D. A Wearable Optical Microfibrous Biomaterial with Encapsulated Nanosensors Enables Wireless Monitoring of Oxidative Stress. *Adv. Funct. Mater.* **2021**, *31*, 2006254.

(68) Wu, H.; Nißler, R.; Morris, V.; Herrmann, N.; Hu, P.; Jeon, S.-J.; Kruss, S.; Giraldo, J. P. Monitoring Plant Health with Near-Infrared Fluorescent H_2O_2 Nanosensors. *Nano Lett.* **2020**, *20*, 2432–2442.

(69) Lew, T. T. S.; Koman, V. B.; Silmore, K. S.; Seo, J. S.; Gordiichuk, P.; Kwak, S.-Y.; Park, M.; Ang, M. C.-Y.; Khong, D. T.; Lee, M. A.; Chan-Park, M. B.; Chua, N.-H.; Strano, M. S. Real-Time Detection of Wound-Induced H2O2 Signalling Waves in Plants with Optical Nanosensors. *Nat. Plants* **2020**, *6*, 404–415.

(70) Hofferber, E. M.; Stapleton, J. A.; Iverson, N. M. Review—Single Walled Carbon Nanotubes as Optical Sensors for Biological Applications. *J. Electrochem. Soc.* **2020**, *167*, 037530.

(71) Zubkovs, V.; Antonucci, A.; Schuergers, N.; Lambert, B.; Latini, A.; Ceccarelli, R.; Santinelli, A.; Rogov, A.; Ciepielewski, D.; Boghossian, A. A. A. Spinning-Disc Confocal Microscopy in the Second near-Infrared Window (NIR-II). *Sci. Rep.* **2018**, *8*, 13770.

(72) Farrera, C.; Torres Andón, F.; Feliu, N. Carbon Nanotubes as Optical Sensors in Biomedicine. *ACS Nano* **2017**, *11*, 10637–10643.

(73) Koman, V. B.; Bakh, N. A.; Jin, X.; Nguyen, F. T.; Son, M.; Kozawa, D.; Lee, M. A.; Bisker, G.; Dong, J.; Strano, M. S. A Wavelength-Induced Frequency Filtering Method for Fluorescent Nanosensors in Vivo. *Nat. Nanotechnol.* **2022**, *17*, 643–652.

(74) Ehrlich, R.; Wulf, V.; Hendler-Neumark, A.; Kagan, B.; Bisker, G. Super-Resolution Radial Fluctuations (SRRF) Nanoscopy in the near Infrared. *Opt. Express* **2022**, *30*.

(75) Kleiner, S.; Wulf, V.; Bisker, G. Single-Walled Carbon Nanotubes as near-Infrared Fluorescent Probes for Bio-Inspired Supramolecular Self-Assembled Hydrogels. *J. Colloid Interface Sci.* **2024**, *670*, 439–448.

(76) Jain, A.; Homayoun, A.; Bannister, C. W.; Yum, K. Single-walled Carbon Nanotubes as Near-infrared Optical Biosensors for Life Sciences and Biomedicine. *Biotechnol. J.* **2015**, *10*, 447–459.

(77) De los Santos, Z. A.; Lin, Z.; Zheng, M. Optical Detection of Stereoselective Interactions with DNA-Wrapped Single-Wall Carbon Nanotubes. *J. Am. Chem.*

Soc. **2021**, *143*, 20628–20632.

(78) Hu, C.; Zhang, Y.; Bao, G.; Zhang, Y.; Liu, M.; Wang, Z. L. DNA Functionalized Single-Walled Carbon Nanotubes for Electrochemical Detection. *J. Phys. Chem. B* **2005**, *109*, 20072–20076.

(79) Zheng, M.; Jagota, A.; Semke, E. D.; Diner, B. A.; Mclean, R. S.; Lustig, S. R.; Richardson, R. E.; Tassi, N. G. DNA-Assisted Dispersion and Separation of Carbon Nanotubes. *Nat. Mater.* **2003**, *2*, 338–342.

(80) Blanch, A. J.; Lenehan, C. E.; Quinton, J. S. Optimizing Surfactant Concentrations for Dispersion of Single-Walled Carbon Nanotubes in Aqueous Solution. *J. Phys. Chem. B* **2010**, *114*, 9805–9811.

(81) Dong, L.; Henderson, A.; Field, C. Antimicrobial Activity of Single-Walled Carbon Nanotubes Suspended in Different Surfactants. *J. Nanotechnol.* **2012**, *2012*, 1–7.

(82) Moore, V. C.; Strano, M. S.; Haroz, E. H.; Hauge, R. H.; Smalley, R. E.; Schmidt, J.; Talmon, Y. Individually Suspended Single-Walled Carbon Nanotubes in Various Surfactants. *Nano Lett.* **2003**, *3*, 1379–1382.

(83) Gerstman, E.; Hendler-Neumark, A.; Wulf, V.; Bisker, G. Monitoring the Formation of Fibrin Clots as Part of the Coagulation Cascade Using Fluorescent Single-Walled Carbon Nanotubes. *ACS Appl. Mater. Interfaces* **2023**, *15*, 21866–21876.

(84) Budhathoki-Uprety, J.; Harvey, J. D. D.; Isaac, E.; Williams, R. M. M.; Galassi, T. V. V.; Langenbacher, R. E. E.; Heller, D. A. A. Polymer Cloaking Modulates the Carbon Nanotube Protein Corona and Delivery into Cancer Cells. *J. Mater. Chem. B* **2017**, *5*, 6637–6644.

(85) Fernandes, R. M. F.; Dai, J.; Regev, O.; Marques, E. F.; Furó, I. Block Copolymers as Dispersants for Single-Walled Carbon Nanotubes: Modes of Surface Attachment and Role of Block Polydispersity. *Langmuir* **2018**, *34*, 13672–13679.

(86) Salalha, W.; Dror, Y.; Khalfin, R. L.; Cohen, Y.; Yarin, A. L.; Zussman, E. Single-Walled Carbon Nanotubes Embedded in Oriented Polymeric Nanofibers by Electrospinning. *Langmuir* **2004**, *20*, 9852–9855.

(87) Antonucci, A.; Kupis-Rozmysłowicz, J.; Boghossian, A. A. Noncovalent Protein and Peptide Functionalization of Single-Walled Carbon Nanotubes for Biodelivery and Optical Sensing Applications. *ACS Appl. Mater. Interfaces* **2017**, *9*, 11321–11331.

(88) Oliveira, S. F.; Bisker, G.; Bakh, N. A.; Gibbs, S. L.; Landry, M. P.; Strano, M. S. Protein Functionalized Carbon Nanomaterials for Biomedical Applications. *Carbon N. Y.* **2015**, *95*, 767–779.

(89) Karajanagi, S. S.; Vertegel, A. A.; Kane, R. S.; Dordick, J. S. Structure and Function of Enzymes Adsorbed onto Single-Walled Carbon Nanotubes. *Langmuir* **2004**, *20*, 11594–11599.

(90) Tsyboulski, D. A.; Bakota, E. L.; Witus, L. S.; Rocha, J.-D. R.; Hartgerink, J. D.; Weisman, R. B. Self-Assembling Peptide Coatings Designed for Highly

Luminescent Suspension of Single-Walled Carbon Nanotubes. *J. Am. Chem. Soc.* **2008**, *130*, 17134–17140.

(91) Abdullah, T. A.; Juzsakova, T.; Hafad, S. A.; Rasheed, R. T.; Al-Jammal, N.; Mallah, M. A.; Salman, A. D.; Le, P. C.; Domokos, E.; Aldulaimi, M. Functionalized Multi-Walled Carbon Nanotubes for Oil Spill Cleanup from Water. *Clean Technol. Environ. Policy* **2022**, *24*, 519–541.

(92) Heller, D. A.; Pratt, G. W.; Zhang, J.; Nair, N.; Hansborough, A. J.; Boghossian, A. A.; Reuel, N. F.; Barone, P. W.; Strano, M. S. Peptide Secondary Structure Modulates Single-Walled Carbon Nanotube Fluorescence as a Chaperone Sensor for Nitroaromatics. *Proc. Natl. Acad. Sci.* **2011**, *108*, 8544–8549.

(93) Matsukawa, Y.; Umemura, K. Chirality Luminescent Properties of Single-Walled Carbon Nanotubes during Redox Reactions. *Opt. Mater. (Amst).* **2021**, *112*, 110748.

(94) Ohno, Y.; Iwasaki, S.; Murakami, Y.; Kishimoto, S.; Maruyama, S.; Mizutani, T. Chirality-Dependent Environmental Effects in Photoluminescence of Single-Walled Carbon Nanotubes. *Phys. Rev. B* **2006**, *73*, 235427.

(95) O'Connell, M. J.; Bachilo, S. M.; Huffman, C. B.; Moore, V. C.; Strano, M. S.; Haroz, E. H.; Rialon, K. L.; Boul, P. J.; Noon, W. H.; Kittrell, C.; Ma, J.; Hauge, R. H.; Weisman, R. B.; Smalley, R. E. Band Gap Fluorescence from Individual Single-Walled Carbon Nanotubes. *Science* **2002**, *297*, 593–596.

(96) Salem, D. P.; Landry, M. P.; Bisker, G.; Ahn, J.; Kruss, S.; Strano, M. S. Chirality Dependent Corona Phase Molecular Recognition of DNA-Wrapped Carbon Nanotubes. *Carbon N. Y.* **2016**, *97*, 147–153.

(97) Choi, J. H.; Strano, M. S. Solvatochromism in Single-Walled Carbon Nanotubes. *Appl. Phys. Lett.* **2007**, *90*, 88–91.

(98) Su, C.; Jiang, L.; Zhang, W. A Review on Heavy Metal Contamination in the Soil Worldwide : Situation , Impact and Remediation Techniques. **2014**, *3*, 24–38.

(99) Järup, L. Hazards of Heavy Metal Contamination. *Br. Med. Bull.* **2003**, *68*, 167–182.

(100) Barnham, K. J.; Bush, A. I. Biological Metals and Metal-Targeting Compounds in Major Neurodegenerative Diseases. *Chem. Soc. Rev* **2014**, *43*, 6727.

(101) Madsen, E.; Gitlin, J. D. Annu. *Rev. Neurosci.2007 30*, 317.

(102) Tofan, L.; Wenkert, R. Chelating Polymers with Valuable Sorption Potential for Development of Precious Metal Recycling Technologies. *Rev. Chem. Eng.* **2022**, *38*, 167–183.

(103) Guo, S.-Y.; Hou, P.-X.; Zhang, F.; Liu, C.; Cheng, H.-M. Gas Sensors Based on Single-Wall Carbon Nanotubes. *Molecules* **2022**, *27*, 5381.

(104) Andjelkovic, M.; Vancamp, J.; Demeulenaer, B.; Depaemelaere, G.; Socaciu, C.; Verloo, M.; Verhe, R. Iron-Chelation Properties of Phenolic Acids Bearing Catechol and Galloyl Groups. *Food Chem.* **2006**, *98*, 23–31.

(105) Irankunda, R.; Camaño Echavarría, J. A.; Paris, C.; Stefan, L.; Desobry, S.; Selmeczi, K.; Muhr, L.; Canabady-Rochelle, L. Metal-Chelating Peptides Separation Using Immobilized Metal Ion Affinity Chromatography: Experimental Methodology and Simulation. *Separations* **2022**, *9*, 370.

(106) Yang, M.; Song, W. J. Diverse Protein Assembly Driven by Metal and Chelating Amino Acids with Selectivity and Tunability. *Nat. Commun.* **2019**, *10*, 5545.

(107) Joshua Ashaolu, T.; Lee, C. C.; Opeolu Ashaolu, J.; Pourjafar, H.; Jafari, S. M. Metal-Binding Peptides and Their Potential to Enhance the Absorption and Bioavailability of Minerals. *Food Chem.* **2023**, *428*, 136678.

(108) Ren, X.; Zou, Q.; Yuan, C.; Chang, R.; Xing, R.; Yan, X. The Dominant Role of Oxygen in Modulating the Chemical Evolution Pathways of Tyrosine in Peptides: Dityrosine or Melanin. *Angew. Chemie* **2019**, *131*, 5930–5934.

(109) Reid, L. O.; Vignoni, M.; Martins-Froment, N.; Thomas, A. H.; Dántola, M. L. Photochemistry of Tyrosine Dimer: When an Oxidative Lesion of Proteins Is Able to Photoinduce Further Damage. *Photochem. Photobiol. Sci.* **2019**, *18*, 1732–1741.

(110) Lampel, A.; McPhee, S. A.; Kassem, S.; Sementa, D.; Massarano, T.; Aramini, J. M.; He, Y.; Ulijn, R. V. Melanin-Inspired Chromophoric Microparticles Composed of Polymeric Peptide Pigments. *Angew. Chemie Int. Ed.* **2021**, *60*, 7564–7569.

(111) Brege, J. J.; Gallaway, C.; Barron, A. R. Fluorescence Quenching of Single-Walled Carbon Nanotubes with Transition-Metal Ions. *J. Phys. Chem. C* **2009**, *113*, 4270–4276.

(112) Settele, S.; Schrage, C. A.; Jung, S.; Michel, E.; Li, H.; Flavel, B. S.; Hashmi, A. S. K.; Kruss, S.; Zaumseil, J. Ratiometric Fluorescent Sensing of Pyrophosphate with Sp^3-Functionalized Single-Walled Carbon Nanotubes. *Nat. Commun.* **2024**, *15*, 706.

(113) Yum, K.; Ahn, J.-H.; McNicholas, T. P.; Barone, P. W.; Mu, B.; Kim, J.-H.; Jain, R. M.; Strano, M. S. Boronic Acid Library for Selective, Reversible Near-Infrared Fluorescence Quenching of Surfactant Suspended Single-Walled Carbon Nanotubes in Response to Glucose. *ACS Nano* **2012**, *6*, 819–830.

(114) O'Connell, M. J.; Eibergen, E. E.; Doorn, S. K. Chiral Selectivity in the Charge-Transfer Bleaching of Single-Walled Carbon-Nanotube Spectra. *Nat. Mater.* **2005**, *4*, 412–418.

(115) Knorr, F. J.; Hung, W.-C.; Wai, C. M. Aromatic Electron Acceptors Change the Chirality Dependence of Single-Walled Carbon Nanotube Oxidation. *Langmuir* **2009**, *25*, 10417–10421.

(116) Satishkumar, B. C.; Brown, L. O.; Gao, Y.; Wang, C.-C.; Wang, H.-L.; Doorn, S. K. Reversible Fluorescence Quenching in Carbon Nanotubes for Biomolecular Sensing. *Nat. Nanotechnol.* **2007**, *2*, 560–564.

(1) Morales, M. A.; Halpern, J. M. Guide to Selecting a Biorecognition Element for Biosensors. *Bioconjug. Chem.* **2018**, *29*, 3231–3239.

(2) Kim, D. C.; Kang, D. J. Molecular Recognition and Specific Interactions for Biosensing Applications. *Sensors* **2008**, *8*, 6605–6641.

(3) Wulf, V.; Bichachi, E.; Hendler-Neumark, A.; Massarano, T.; Leshem, A. B.; Lampel, A.; Bisker, G.; Hendler-Neumark, A.; Massarano, T.; Leshem, A. B.; Lampel, A.; Bisker, G. Multicomponent System of Single-Walled Carbon Nanotubes Functionalized with a Melanin-Inspired Material for Optical Detection and Scavenging of Metals. *Adv. Funct. Mater.* **2022**, *32*, 2209688.

(4) Blake, D. A.; Jones, R. M.; Blake, R. C.; Pavlov, A. R.; Darwish, I. A.; Yu, H. Antibody-Based Sensors for Heavy Metal Ions. *Biosens. Bioelectron.* **2001**, *16*, 799–809.

(5) Carter, K. P.; Young, A. M.; Palmer, A. E. Fluorescent Sensors for Measuring Metal Ions in Living Systems. *Chem. Rev.* **2014**, *114*, 4564–4601.

(6) El-Safty, S. A.; Prabhakaran, D.; Ismail, A. A.; Matsunaga, H.; Mizukami, F. Nanosensor Design Packages: A Smart and Compact Development for Metal Ions Sensing Responses. *Adv. Funct. Mater.* **2007**, *17*, 3731–3745.

(7) Zhang, L.; Peng, D.; Liang, R.-P.; Qiu, J.-D. Graphene-Based Optical Nanosensors for Detection of Heavy Metal Ions. *TrAC Trends Anal. Chem.* **2018**, *102*, 280–289.

(8) Cho, E. J.; Lee, J.-W.; Ellington, A. D. Applications of Aptamers as Sensors. *Annu. Rev. Anal. Chem.* **2009**, *2*, 241–264.

(9) Byrne, B.; Stack, E.; Gilmartin, N.; O'Kennedy, R. Antibody-Based Sensors: Principles, Problems and Potential for Detection of Pathogens and Associated Toxins. *Sensors* **2009**, *9*, 4407–4445.

(10) Nguyen, H. H.; Lee, S. H.; Lee, U. J.; Fermin, C. D.; Kim, M. Immobilized Enzymes in Biosensor Applications. *Materials (Basel).* **2019**, *12*, 121.

(11) Zhang, J.; Landry, M. P.; Barone, P. W.; Kim, J.-H.; Lin, S.; Ulissi, Z. W.; Lin, D.; Mu, B.; Boghossian, A. A.; Hilmer, A. J.; Rwei, A.; Hinckley, A. C.; Kruss, S.; Shandell, M. A.; Nair, N.; Blake, S.; Şen, F.; Şen, S.; Croy, R. G.; Li, D.; Yum, K.; Ahn, J.-H.; Jin, H.; Heller, D. A.; Essigmann, J. M.; Blankschtein, D.; Strano, M. S. Molecular Recognition Using Corona Phase Complexes Made of Synthetic Polymers Adsorbed on Carbon Nanotubes. *Nat. Nanotechnol.* **2013**, *8*, 959–968.

(12) Bisker, G.; Dong, J.; Park, H. D.; Iverson, N. M.; Ahn, J.; Nelson, J. T.; Landry, M. P.; Kruss, S.; Strano, M. S. Protein-Targeted Corona Phase Molecular Recognition. *Nat. Commun.* **2016**, *7*, 10241.

(13) Yotova, L.; Yaneva, S.; Marinkova, D. Biomimetic Nanosensors for Determination of Toxic Compounds in Food and Agricultural Products (Review). *J. Univ. Chem. Technol. Metall.* **2013**, *48*, 215–227.

(14) Denizli, A. Molecular Imprinting for Nanosensors and Other Sensing Applications. *Mol. Imprinting Nanosensors Other Sens. Appl.* **2021**, 1–417.

(15) Adampourezare, M.; Nikzad, B.; Nasrollahzadeh, S.; Asadpour-Zeynali, K.; de la Guardia, M.; Ezzati Nazhad Dolatabadi, J.; Zhang, F.; Mahdi Jafari, S. Polysaccharide-Based Sensors and Nanosensors: A Review of Recent Progress

and Challenges. *Microchem. J.* **2024**, *204*, 110944.

(16) Nocerino, V.; Miranda, B.; Tramontano, C.; Chianese, G.; Dardano, P.; Rea, I.; De Stefano, L. Plasmonic Nanosensors: Design, Fabrication, and Applications in Biomedicine. *Chemosensors* **2022**, *10*, 150.

(17) Zhang, L.; Yang, Y.; Tan, J.; Yuan, Q. Chemically Modified Nucleic Acid Biopolymers Used in Biosensing. *Mater. Chem. Front.* **2020**, *4*, 1315–1327.

(18) Shumeiko, V.; Zaken, Y.; Hidas, G.; Paltiel, Y.; Bisker, G.; Shoseyov, O. Peptide-Encapsulated Single-Wall Carbon Nanotube-Based Near-Infrared Optical Nose for Bacteria Detection and Classification. *IEEE Sens. J.* **2022**, *22*, 6277–6287.

(19) Zong, C.; Fang, L.; Song, F.; Wang, A.; Wan, Y. Fluorescent Fingerprint Bacteria by Multi-Channel Magnetic Fluorescent Nanosensor. *Sensors Actuators B Chem.* **2019**, *289*, 234–241.

(20) Amir, D.; Hendler-Neumark, A.; Wulf, V.; Ehrlich, R.; Bisker, G. Oncometabolite Fingerprinting Using Fluorescent Single-Walled Carbon Nanotubes. *Adv. Mater. Interfaces* **2022**, *9*.

(21) Kim, M.; Chen, C.; Wang, P.; Mulvey, J. J.; Yang, Y.; Wun, C.; Antman-Passig, M.; Luo, H.-B.; Cho, S.; Long-Roche, K.; Ramanathan, L. V.; Jagota, A.; Zheng, M.; Wang, Y.; Heller, D. A. Detection of Ovarian Cancer via the Spectral Fingerprinting of Quantum-Defect-Modified Carbon Nanotubes in Serum by Machine Learning. *Nat. Biomed. Eng.* **2022**, *6*, 267–275.

(22) Nißler, R.; Bader, O.; Dohmen, M.; Walter, S. G.; Noll, C.; Selvaggio, G.; Groß, U.; Kruss, S. Remote near Infrared Identification of Pathogens with Multiplexed Nanosensors. *Nat. Commun.* **2020**, *11*, 5995.

(23) Ebrahim-Habibi, M.-B.; Ghobeh, M.; Mahyari, F. A.; Rafii-Tabar, H.; Sasanpour, P. An Investigation into Non-Covalent Functionalization of a Single-Walled Carbon Nanotube and a Graphene Sheet with Protein G:A Combined Experimental and Molecular Dynamics Study. *Sci. Rep.* **2019**, *9*, 1273.

(24) Sultana, N.; Dewey, H. M.; Arellano, A. G.; Budhathoki-Uprety, J. Understanding the Molecular Assemblies of Single Walled Carbon Nanotubes and Tailoring Their Photoluminescence for the Next-Generation Optical Nanosensors. *Chem. Mater.* **2024**, *36*, 4034–4053.

(25) Ramezani, F.; Rafii-Tabar, H. An In-Depth View of Human Serum Albumin Corona on Gold Nanoparticles. *Mol. Biosyst.* **2015**, *11*, 454–462.

(26) Zuo, G.; Zhou, X.; Huang, Q.; Fang, H.; Zhou, R. Adsorption of Villin Headpiece onto Graphene, Carbon Nanotube, and C60: Effect of Contacting Surface Curvatures on Binding Affinity. *J. Phys. Chem. C* **2011**, *115*, 23323–23328.

(27) Harrison, E. T.; Weidner, T.; Castner, D. G.; Interlandi, G. Predicting the Orientation of Protein G B1 on Hydrophobic Surfaces Using Monte Carlo Simulations. *Biointerphases* **2017**, *12*.

(28) Xiao, H.; Huang, B.; Yao, G.; Kang, W.; Gong, S.; Pan, H.; Cao, Y.; Wang, J.;

Zhang, J.; Wang, W. Atomistic Simulation of the Coupled Adsorption and Unfolding of Protein GB1 on the Polystyrenes Nanoparticle Surface. *Sci. China Physics, Mech. Astron.* **2018**, *61*, 038711.

(29) Lambert, B. P.; Taheri, A.; Wu, S.-J.; Gillen, A. J.; Kashaninejad, M.; Boghossian, A. A. Directed Evolution of Nanosensors for the Detection of Mycotoxins. *bioRxiv*. June 14, 2023.

(30) An, S.; Suh, Y.; Kelich, P.; Lee, D.; Vukovic, L.; Jeong, S. Directed Evolution of Near-Infrared Serotonin Nanosensors with Machine Learning-Based Screening. *Nanomaterials* **2024**, *14*, 247.

(31) Jeong, S.; Yang, D.; Beyene, A. G. G.; Del Bonis-O'Donnell, J. T. T.; Gest, A. M. M. M. M.; Navarro, N.; Sun, X.; Landry, M. P. P. High-Throughput Evolution of near-Infrared Serotonin Nanosensors. *Sci. Adv.* **2019**, *5*, eaay3771.

(32) Conroy, P. J.; Hearty, S.; Leonard, P.; O'Kennedy, R. J. Antibody Production, Design and Use for Biosensor-Based Applications. *Semin. Cell Dev. Biol.* **2009**, *20*, 10–26.

(33) Bettinger, H. F. Carbon Nanotubes—Basic Concepts and Physical Properties. By S. Reich, C. Thomsen, J. Maultzsch. *ChemPhysChem* **2004**, *5*, 1914–1915.

(34) Kruss, S.; Hilmer, A. J.; Zhang, J.; Reuel, N. F.; Mu, B.; Strano, M. S. Carbon Nanotubes as Optical Biomedical Sensors. *Adv. Drug Deliv. Rev.* **2013**, *65*, 1933–1950.

(35) Bachilo, S. M.; Strano, M. S.; Kittrell, C.; Hauge, R. H.; Smalley, R. E.; Weisman, R. B. Structure-Assigned Optical Spectra of Single-Walled Carbon Nanotubes. *Science* **2002**, *298*, 2361–2366.

(36) Ackermann, J.; Metternich, J. T.; Herbertz, S.; Kruss, S. Biosensing with Fluorescent Carbon Nanotubes. *Angew. Chemie Int. Ed.* **2022**, *61*, e202112372.

(37) Weisman, R. B.; Bachilo, S. M. Dependence of Optical Transition Energies on Structure for Single-Walled Carbon Nanotubes in Aqueous Suspension: An Empirical Kataura Plot. *Nano Lett.* **2003**, *3*, 1235–1238.

(38) Qiu, L.; Ding, F. Understanding Single-Walled Carbon Nanotube Growth for Chirality Controllable Synthesis. *Accounts Mater. Res.* **2021**, *2*, 828–841.

(39) Irita, M.; Yamamoto, T.; Homma, Y. Chirality Distributions for Semiconducting Single-Walled Carbon Nanotubes Determined by Photoluminescence Spectroscopy. *Nanomaterials* **2021**, *11*, 2309.

(40) Bonis-O'Donnell, J. T. Del; Page, R. H.; Beyene, A. G.; Tindall, E. G.; McFarlane, I. R.; Landry, M. P. Dual Near-Infrared Two-Photon Microscopy for Deep-Tissue Dopamine Nanosensor Imaging. *Adv. Funct. Mater.* **2017**, *27*.

(41) Iverson, N. M.; Barone, P. W.; Shandell, M.; Trudel, L. J.; Sen, S.; Sen, F.; Ivanov, V.; Atolia, E.; Farias, E.; McNicholas, T. P.; Reuel, N.; Parry, N. M. A.; Wogan, G. N.; Strano, M. S. In Vivo Biosensing via Tissue-Localizable near-Infrared-Fluorescent Single-Walled Carbon Nanotubes. *Nat. Nanotechnol.* **2013**, *8*, 873–880.

(42) Hendler-Neumark, A.; Wulf, V.; Bisker, G. In Vivo Imaging of Fluorescent

Single-Walled Carbon Nanotubes within C. Elegans Nematodes in the near-Infrared Window. *Mater. Today Bio* **2021**, *12*, 100175.

(43) Iverson, N. M.; Bisker, G.; Farias, E.; Ivanov, V.; Ahn, J.; Wogan, G. N.; Strano, M. S. Quantitative Tissue Spectroscopy of Near Infrared Fluorescent Nanosensor Implants. *J. Biomed. Nanotechnol.* **2016**, *12*, 1035–1047.

(44) Nandi, S.; Caicedo, K.; Cognet, L. When Super-Resolution Localization Microscopy Meets Carbon Nanotubes. *Nanomaterials* **2022**, *12*, 1433.

(45) Barone, P. W.; Baik, S.; Heller, D. A.; Strano, M. S. Near-Infrared Optical Sensors Based on Single-Walled Carbon Nanotubes. *Nat. Mater.* **2005**, *4*, 86–92.

(46) Boghossian, A. A.; Zhang, J.; Barone, P. W.; Reuel, N. F.; Kim, J.; Heller, D. A.; Ahn, J.; Hilmer, A. J.; Rwei, A.; Arkalgud, J. R.; Zhang, C. T.; Strano, M. S. Near-Infrared Fluorescent Sensors Based on Single-Walled Carbon Nanotubes for Life Sciences Applications. *ChemSusChem* **2011**, *4*, 848–863.

(47) Nißler, R.; Ackermann, J.; Ma, C.; Kruss, S. Prospects of Fluorescent Single-Chirality Carbon Nanotube-Based Biosensors. *Anal. Chem.* **2022**, *94*, 9941–9951.

(48) Zhang, Y.; Guo, J.; Tang, Z.; Tang, C.; Li, Y.; Tao, X.; Zhou, B.; Chen, W.; Guo, L.; Tang, K.; Liang, T. Recent Developments and Trends of Biosensors Based on Carbon Nanotubes for Biomedical Diagnosis Applications: A Review. *Biosens. Bioelectron. X* **2024**, *17*, 100424.

(49) Murjani, B. O.; Kadu, P. S.; Bansod, M.; Vaidya, S. S.; Yadav, M. D. Carbon Nanotubes in Biomedical Applications: Current Status, Promises, and Challenges. *Carbon Lett.* **2022**, *32*, 1207–1226.

(50) Acharya, R.; Patil, T. V.; Dutta, S. D.; Lee, J.; Ganguly, K.; Kim, H.; Randhawa, A.; Lim, K. Single-Walled Carbon Nanotube-Based Optical Nano/Biosensors for Biomedical Applications: Role in Bioimaging, Disease Diagnosis, and Biomarkers Detection. *Adv. Mater. Technol.* **2024**, 2400279.

(51) Yaari, Z.; Cheung, J. M.; Baker, H. A.; Frederiksen, R. S.; Jena, P. V.; Horoszko, C. P.; Jiao, F.; Scheuring, S.; Luo, M.; Heller, D. A. Nanoreporter of an Enzymatic Suicide Inactivation Pathway. *Nano Lett.* **2020**, *20*, 7819–7827.

(52) Kallmyer, N. E.; Abdennadher, M. S.; Agarwal, S.; Baldwin-Kordick, R.; Khor, R. L.; Kooistra, A. S.; Peterson, E.; McDaniel, M. D.; Reuel, N. F. Inexpensive Near-Infrared Fluorimeters: Enabling Translation of NIR-Based Assays to the Field. *Anal. Chem.* **2021**, *93*, 4800–4808.

(53) Dong, J.; Lee, M. A. A.; Rajan, A. G. G.; Rahaman, I.; Sun, J. H. H.; Park, M.; Salem, D. P. P.; Strano, M. S. S. A Synthetic Mimic of Phosphodiesterase Type 5 Based on Corona Phase Molecular Recognition of Single-Walled Carbon Nanotubes. *Proc. Natl. Acad. Sci.* **2020**, *117*.

(54) Wulf, V.; Slor, G.; Rathee, P.; Amir, R. J.; Bisker, G. Dendron–Polymer Hybrids as Tailorable Responsive Coronae of Single-Walled Carbon Nanotubes. *ACS Nano* **2021**, *15*, 20539–20549.

(55) Basu, S.; Hendler-Neumark, A.; Bisker, G. Rationally Designed

Functionalization of Single-Walled Carbon Nanotubes for Real-Time Monitoring of Cholinesterase Activity and Inhibition in Plasma. *Small* **2024**, *20*.

(56) Basu, S.; Hendler-Neumark, A.; Bisker, G. Monitoring Enzyme Activity Using Near-Infrared Fluorescent Single-Walled Carbon Nanotubes. *ACS Sensors* **2024**, *9*, 2237–2253.

(57) Williams, R. M.; Harvey, J. D.; Budhathoki-Uprety, J.; Heller, D. A. Glutathione-S-Transferase Fusion Protein Nanosensor. *Nano Lett.* **2020**, *20*, 7287–7295.

(58) Ehrlich, R.; Hendler-Neumark, A.; Wulf, V.; Amir, D.; Bisker, G. Optical Nanosensors for Real-Time Feedback on Insulin Secretion by B-Cells. *Small* **2021**, *17*, 2101660.

(59) Pinals, R. L.; Ledesma, F.; Yang, D.; Navarro, N.; Jeong, S.; Pak, J. E.; Kuo, L.; Chuang, Y.-C.; Cheng, Y.-W.; Sun, H.-Y.; Landry, M. P. Rapid SARS-CoV-2 Spike Protein Detection by Carbon Nanotube-Based Near-Infrared Nanosensors. *Nano Lett.* **2021**, *21*, 2272–2280.

(60) Nelson, J. T.; Kim, S.; Reuel, N. F.; Salem, D. P.; Bisker, G.; Landry, M. P.; Kruss, S.; Barone, P. W.; Kwak, S.; Strano, M. S. Mechanism of Immobilized Protein A Binding to Immunoglobulin G on Nanosensor Array Surfaces. *Anal. Chem.* **2015**, *87*, 8186–8193.

(61) Gillen, A. J.; Siefman, D. J.; Wu, S.-J.; Bourmaud, C.; Lambert, B.; Boghossian, A. A. Templating Colloidal Sieves for Tuning Nanotube Surface Interactions and Optical Sensor Responses. *J. Colloid Interface Sci.* **2020**, *565*, 55–62.

(62) Kruss, S.; Landry, M. P.; Vander Ende, E.; Lima, B. M. A.; Reuel, N. F.; Zhang, J.; Nelson, J.; Mu, B.; Hilmer, A.; Strano, M. Neurotransmitter Detection Using Corona Phase Molecular Recognition on Fluorescent Single-Walled Carbon Nanotube Sensors. *J. Am. Chem. Soc.* **2014**, *136*, 713–724.

(63) Beyene, A. G. G.; Delevich, K.; Del Bonis-O'Donnell, J. T. T.; Piekarski, D. J. J.; Lin, W. C. C.; Thomas, A. W. W.; Yang, S. J. J.; Kosillo, P.; Yang, D.; Prounis, G. S. S.; Wilbrecht, L.; Landry, M. P. P. Imaging Striatal Dopamine Release Using a Nongenetically Encoded near Infrared Fluorescent Catecholamine Nanosensor. *Sci. Adv.* **2019**, *5*, eaaw3108.

(64) Dinarvand, M.; Elizarova, S.; Daniel, J.; Kruss, S. Imaging of Monoamine Neurotransmitters with Fluorescent Nanoscale Sensors. *Chempluschem* **2020**, *85*, 1465–1480.

(65) Lee, M. A.; Wang, S.; Jin, X.; Bakh, N. A.; Nguyen, F. T.; Dong, J.; Silmore, K. S.; Gong, X.; Pham, C.; Jones, K. K.; Muthupalani, S.; Bisker, G.; Son, M.; Strano, M. S. Implantable Nanosensors for Human Steroid Hormone Sensing In Vivo Using a Self-Templating Corona Phase Molecular Recognition. *Adv. Healthc. Mater.* **2020**, *9*.

(66) Wong, M. H.; Giraldo, J. P.; Kwak, S.-Y.; Koman, V. B.; Sinclair, R.; Lew, T. T. S.; Bisker, G.; Liu, P.; Strano, M. S. Nitroaromatic Detection and Infrared Communication from Wild-Type Plants Using Plant Nanobionics. *Nat. Mater.*

2017, *16*, 264–272.

(67) Safaee, M. M. M.; Gravely, M.; Roxbury, D. A Wearable Optical Microfibrous Biomaterial with Encapsulated Nanosensors Enables Wireless Monitoring of Oxidative Stress. *Adv. Funct. Mater.* **2021**, *31*, 2006254.

(68) Wu, H.; Nißler, R.; Morris, V.; Herrmann, N.; Hu, P.; Jeon, S.-J.; Kruss, S.; Giraldo, J. P. Monitoring Plant Health with Near-Infrared Fluorescent H_2O_2 Nanosensors. *Nano Lett.* **2020**, *20*, 2432–2442.

(69) Lew, T. T. S.; Koman, V. B.; Silmore, K. S.; Seo, J. S.; Gordiichuk, P.; Kwak, S.-Y.; Park, M.; Ang, M. C.-Y.; Khong, D. T.; Lee, M. A.; Chan-Park, M. B.; Chua, N.-H.; Strano, M. S. Real-Time Detection of Wound-Induced H2O2 Signalling Waves in Plants with Optical Nanosensors. *Nat. Plants* **2020**, *6*, 404–415.

(70) Hofferber, E. M.; Stapleton, J. A.; Iverson, N. M. Review—Single Walled Carbon Nanotubes as Optical Sensors for Biological Applications. *J. Electrochem. Soc.* **2020**, *167*, 037530.

(71) Zubkovs, V.; Antonucci, A.; Schuergers, N.; Lambert, B.; Latini, A.; Ceccarelli, R.; Santinelli, A.; Rogov, A.; Ciepielewski, D.; Boghossian, A. A. A. Spinning-Disc Confocal Microscopy in the Second near-Infrared Window (NIR-II). *Sci. Rep.* **2018**, *8*, 13770.

(72) Farrera, C.; Torres Andón, F.; Feliu, N. Carbon Nanotubes as Optical Sensors in Biomedicine. *ACS Nano* **2017**, *11*, 10637–10643.

(73) Koman, V. B.; Bakh, N. A.; Jin, X.; Nguyen, F. T.; Son, M.; Kozawa, D.; Lee, M. A.; Bisker, G.; Dong, J.; Strano, M. S. A Wavelength-Induced Frequency Filtering Method for Fluorescent Nanosensors in Vivo. *Nat. Nanotechnol.* **2022**, *17*, 643–652.

(74) Ehrlich, R.; Wulf, V.; Hendler-Neumark, A.; Kagan, B.; Bisker, G. Super-Resolution Radial Fluctuations (SRRF) Nanoscopy in the near Infrared. *Opt. Express* **2022**, *30*.

(75) Kleiner, S.; Wulf, V.; Bisker, G. Single-Walled Carbon Nanotubes as near-Infrared Fluorescent Probes for Bio-Inspired Supramolecular Self-Assembled Hydrogels. *J. Colloid Interface Sci.* **2024**, *670*, 439–448.

(76) Jain, A.; Homayoun, A.; Bannister, C. W.; Yum, K. Single-walled Carbon Nanotubes as Near-infrared Optical Biosensors for Life Sciences and Biomedicine. *Biotechnol. J.* **2015**, *10*, 447–459.

(77) De los Santos, Z. A.; Lin, Z.; Zheng, M. Optical Detection of Stereoselective Interactions with DNA-Wrapped Single-Wall Carbon Nanotubes. *J. Am. Chem. Soc.* **2021**, *143*, 20628–20632.

(78) Hu, C.; Zhang, Y.; Bao, G.; Zhang, Y.; Liu, M.; Wang, Z. L. DNA Functionalized Single-Walled Carbon Nanotubes for Electrochemical Detection. *J. Phys. Chem. B* **2005**, *109*, 20072–20076.

(79) Zheng, M.; Jagota, A.; Semke, E. D.; Diner, B. A.; Mclean, R. S.; Lustig, S. R.; Richardson, R. E.; Tassi, N. G. DNA-Assisted Dispersion and Separation of Carbon Nanotubes. *Nat. Mater.* **2003**, *2*, 338–342.

(80) Blanch, A. J.; Lenehan, C. E.; Quinton, J. S. Optimizing Surfactant Concentrations for Dispersion of Single-Walled Carbon Nanotubes in Aqueous Solution. *J. Phys. Chem. B* **2010**, *114*, 9805–9811.

(81) Dong, L.; Henderson, A.; Field, C. Antimicrobial Activity of Single-Walled Carbon Nanotubes Suspended in Different Surfactants. *J. Nanotechnol.* **2012**, *2012*, 1–7.

(82) Moore, V. C.; Strano, M. S.; Haroz, E. H.; Hauge, R. H.; Smalley, R. E.; Schmidt, J.; Talmon, Y. Individually Suspended Single-Walled Carbon Nanotubes in Various Surfactants. *Nano Lett.* **2003**, *3*, 1379–1382.

(83) Gerstman, E.; Hendler-Neumark, A.; Wulf, V.; Bisker, G. Monitoring the Formation of Fibrin Clots as Part of the Coagulation Cascade Using Fluorescent Single-Walled Carbon Nanotubes. *ACS Appl. Mater. Interfaces* **2023**, *15*, 21866–21876.

(84) Budhathoki-Uprety, J.; Harvey, J. D. D.; Isaac, E.; Williams, R. M. M.; Galassi, T. V. V.; Langenbacher, R. E. E.; Heller, D. A. A. Polymer Cloaking Modulates the Carbon Nanotube Protein Corona and Delivery into Cancer Cells. *J. Mater. Chem. B* **2017**, *5*, 6637–6644.

(85) Fernandes, R. M. F.; Dai, J.; Regev, O.; Marques, E. F.; Furó, I. Block Copolymers as Dispersants for Single-Walled Carbon Nanotubes: Modes of Surface Attachment and Role of Block Polydispersity. *Langmuir* **2018**, *34*, 13672–13679.

(86) Salalha, W.; Dror, Y.; Khalfin, R. L.; Cohen, Y.; Yarin, A. L.; Zussman, E. Single-Walled Carbon Nanotubes Embedded in Oriented Polymeric Nanofibers by Electrospinning. *Langmuir* **2004**, *20*, 9852–9855.

(87) Antonucci, A.; Kupis-Rozmysłowicz, J.; Boghossian, A. A. Noncovalent Protein and Peptide Functionalization of Single-Walled Carbon Nanotubes for Biodelivery and Optical Sensing Applications. *ACS Appl. Mater. Interfaces* **2017**, *9*, 11321–11331.

(88) Oliveira, S. F.; Bisker, G.; Bakh, N. A.; Gibbs, S. L.; Landry, M. P.; Strano, M. S. Protein Functionalized Carbon Nanomaterials for Biomedical Applications. *Carbon N. Y.* **2015**, *95*, 767–779.

(89) Karajanagi, S. S.; Vertegel, A. A.; Kane, R. S.; Dordick, J. S. Structure and Function of Enzymes Adsorbed onto Single-Walled Carbon Nanotubes. *Langmuir* **2004**, *20*, 11594–11599.

(90) Tsyboulski, D. A.; Bakota, E. L.; Witus, L. S.; Rocha, J.-D. R.; Hartgerink, J. D.; Weisman, R. B. Self-Assembling Peptide Coatings Designed for Highly Luminescent Suspension of Single-Walled Carbon Nanotubes. *J. Am. Chem. Soc.* **2008**, *130*, 17134–17140.

(91) Abdullah, T. A.; Juzsakova, T.; Hafad, S. A.; Rasheed, R. T.; Al-Jammal, N.; Mallah, M. A.; Salman, A. D.; Le, P. C.; Domokos, E.; Aldulaimi, M. Functionalized Multi-Walled Carbon Nanotubes for Oil Spill Cleanup from Water. *Clean Technol. Environ. Policy* **2022**, *24*, 519–541.

(92) Heller, D. A.; Pratt, G. W.; Zhang, J.; Nair, N.; Hansborough, A. J.;

Boghossian, A. A.; Reuel, N. F.; Barone, P. W.; Strano, M. S. Peptide Secondary Structure Modulates Single-Walled Carbon Nanotube Fluorescence as a Chaperone Sensor for Nitroaromatics. *Proc. Natl. Acad. Sci.* **2011**, *108*, 8544–8549.

(93) Matsukawa, Y.; Umemura, K. Chirality Luminescent Properties of Single-Walled Carbon Nanotubes during Redox Reactions. *Opt. Mater. (Amst).* **2021**, *112*, 110748.

(94) Ohno, Y.; Iwasaki, S.; Murakami, Y.; Kishimoto, S.; Maruyama, S.; Mizutani, T. Chirality-Dependent Environmental Effects in Photoluminescence of Single-Walled Carbon Nanotubes. *Phys. Rev. B* **2006**, *73*, 235427.

(95) O'Connell, M. J.; Bachilo, S. M.; Huffman, C. B.; Moore, V. C.; Strano, M. S.; Haroz, E. H.; Rialon, K. L.; Boul, P. J.; Noon, W. H.; Kittrell, C.; Ma, J.; Hauge, R. H.; Weisman, R. B.; Smalley, R. E. Band Gap Fluorescence from Individual Single-Walled Carbon Nanotubes. *Science* **2002**, *297*, 593–596.

(96) Salem, D. P.; Landry, M. P.; Bisker, G.; Ahn, J.; Kruss, S.; Strano, M. S. Chirality Dependent Corona Phase Molecular Recognition of DNA-Wrapped Carbon Nanotubes. *Carbon N. Y.* **2016**, *97*, 147–153.

(97) Choi, J. H.; Strano, M. S. Solvatochromism in Single-Walled Carbon Nanotubes. *Appl. Phys. Lett.* **2007**, *90*, 88–91.

(98) Su, C.; Jiang, L.; Zhang, W. A Review on Heavy Metal Contamination in the Soil Worldwide : Situation , Impact and Remediation Techniques. **2014**, *3*, 24–38.

(99) Järup, L. Hazards of Heavy Metal Contamination. *Br. Med. Bull.* **2003**, *68*, 167–182.

(100) Barnham, K. J.; Bush, A. I. Biological Metals and Metal-Targeting Compounds in Major Neurodegenerative Diseases. *Chem. Soc. Rev* **2014**, *43*, 6727.

(101) Madsen, E.; Gitlin, J. D. Annu. *Rev. Neurosci.2007 30*, 317.

(102) Tofan, L.; Wenkert, R. Chelating Polymers with Valuable Sorption Potential for Development of Precious Metal Recycling Technologies. *Rev. Chem. Eng.* **2022**, *38*, 167–183.

(103) Guo, S.-Y.; Hou, P.-X.; Zhang, F.; Liu, C.; Cheng, H.-M. Gas Sensors Based on Single-Wall Carbon Nanotubes. *Molecules* **2022**, *27*, 5381.

(104) Andjelkovic, M.; Vancamp, J.; Demeulenaer, B.; Depaemelaere, G.; Socaciu, C.; Verloo, M.; Verhe, R. Iron-Chelation Properties of Phenolic Acids Bearing Catechol and Galloyl Groups. *Food Chem.* **2006**, *98*, 23–31.

(105) Irankunda, R.; Camaño Echavarría, J. A.; Paris, C.; Stefan, L.; Desobry, S.; Selmeczi, K.; Muhr, L.; Canabady-Rochelle, L. Metal-Chelating Peptides Separation Using Immobilized Metal Ion Affinity Chromatography: Experimental Methodology and Simulation. *Separations* **2022**, *9*, 370.

(106) Yang, M.; Song, W. J. Diverse Protein Assembly Driven by Metal and Chelating Amino Acids with Selectivity and Tunability. *Nat. Commun.* **2019**, *10*, 5545.

(107) Joshua Ashaolu, T.; Lee, C. C.; Opeolu Ashaolu, J.; Pourjafar, H.; Jafari, S. M. Metal-Binding Peptides and Their Potential to Enhance the Absorption and Bioavailability of Minerals. *Food Chem.* **2023**, *428*, 136678.

(108) Ren, X.; Zou, Q.; Yuan, C.; Chang, R.; Xing, R.; Yan, X. The Dominant Role of Oxygen in Modulating the Chemical Evolution Pathways of Tyrosine in Peptides: Dityrosine or Melanin. *Angew. Chemie* **2019**, *131*, 5930–5934.

(109) Reid, L. O.; Vignoni, M.; Martins-Froment, N.; Thomas, A. H.; Dántola, M. L. Photochemistry of Tyrosine Dimer: When an Oxidative Lesion of Proteins Is Able to Photoinduce Further Damage. *Photochem. Photobiol. Sci.* **2019**, *18*, 1732–1741.

(110) Lampel, A.; McPhee, S. A.; Kassem, S.; Sementa, D.; Massarano, T.; Aramini, J. M.; He, Y.; Ulijn, R. V. Melanin-Inspired Chromophoric Microparticles Composed of Polymeric Peptide Pigments. *Angew. Chemie Int. Ed.* **2021**, *60*, 7564–7569.

(111) Brege, J. J.; Gallaway, C.; Barron, A. R. Fluorescence Quenching of Single-Walled Carbon Nanotubes with Transition-Metal Ions. *J. Phys. Chem. C* **2009**, *113*, 4270–4276.

(112) Settele, S.; Schrage, C. A.; Jung, S.; Michel, E.; Li, H.; Flavel, B. S.; Hashmi, A. S. K.; Kruss, S.; Zaumseil, J. Ratiometric Fluorescent Sensing of Pyrophosphate with Sp^3-Functionalized Single-Walled Carbon Nanotubes. *Nat. Commun.* **2024**, *15*, 706.

(113) Yum, K.; Ahn, J.-H.; McNicholas, T. P.; Barone, P. W.; Mu, B.; Kim, J.-H.; Jain, R. M.; Strano, M. S. Boronic Acid Library for Selective, Reversible Near-Infrared Fluorescence Quenching of Surfactant Suspended Single-Walled Carbon Nanotubes in Response to Glucose. *ACS Nano* **2012**, *6*, 819–830.

(114) O'Connell, M. J.; Eibergen, E. E.; Doorn, S. K. Chiral Selectivity in the Charge-Transfer Bleaching of Single-Walled Carbon-Nanotube Spectra. *Nat. Mater.* **2005**, *4*, 412–418.

(115) Knorr, F. J.; Hung, W.-C.; Wai, C. M. Aromatic Electron Acceptors Change the Chirality Dependence of Single-Walled Carbon Nanotube Oxidation. *Langmuir* **2009**, *25*, 10417–10421.

(116) Satishkumar, B. C.; Brown, L. O.; Gao, Y.; Wang, C.-C.; Wang, H.-L.; Doorn, S. K. Reversible Fluorescence Quenching in Carbon Nanotubes for Biomolecular Sensing. *Nat. Nanotechnol.* **2007**, *2*, 560–564.

6. תקציר

מתכות כבדות מהוות סכנה משמעותית לבריאות האדם ולסביבה. יכולתן של מתכות כבדות להצטבר ביצורים חיים היא הסיבה לרעילותם הגבוהה שכן הן עלולות לגרום לבעיות רפואיות חמורות כגון מחלות נוירולוגיות, נזקים לכליות, וסוגים שונים של סרטן. בהשראת אתרי קישור טבעיים של יוני מתכת הנוצרים על ידי קבוצות פונקציונליות ספציפיות של חומצות האמינו באנזימים וחלבונים, פיתחנו סט של ננו-צינוריות פחמן חד-שכבתיות (Single-walled carbon nanotubes) עטופות בפפטידים, המשמשות כחיישנים פלורסנטיים בטווח האינפרה אדום הקרוב, בעלי תאימות ביולוגית, עבור זיהוי של יוני מתכת. ספריית חיישנים זו מכילה חיישנים המאוקטבים על ידי רצפים ייחודיים של חומצות אמינו שביניהן חומצות אמינו המיועדות לקשירת מתכות. חיישנים אלו מגלים דפוסי תגובה אופטית מגוונים עבור מספר יוני מתכת שנבדקו. לצורך הגדלת מספר החיישנים בספריה, והרחבת הגיוון שלהם, אנו משתמשים בכירליות השונות של ננו-צינוריות הפחמן החד-שכבתיות. נוסף על כך, אנו מבצעים שינויים כימיים של הפפטידים העוטפים את הסנסורים באמצעות פוטוכימיה. ננו-צינוריות הפחמן החד-שכבתיות העטופות בפפטידים, המרכיבות את סט חיישנים, מאפשרות זיהוי של יוני מתכת כבדים על ידי ניתוח דפוסי התגובה הפלורסנטית. קלות הסינתזה של המערכת ומגוון הפפטידים בה מקדם יצירת סטים של חיישנים פלורסנטיים בטווח האינפרה אדום הקרוב עבור מגוון רחב של אנליטים וסביבות שונים.

אוניברסיטת תל – אביב

הפקולטה להנדסה ע"ש איבי ואלדר פליישמן

בית הספר לתארים מתקדמים ע"ש זנדמן-סליינר

זיהוי מתכות כבדות באמצעות ננו-צינוריות פחמן חד-שכבתיות עטופות בפפטידים המשמשות כחיישנים אופטיים

חיבור זה הוגש כעבודת גמר לקראת התואר "מוסמך אוניברסיטה" בהנדסה ביו-רפואית

על-ידי

גבריאל פטרסקי

העבודה נעשתה במחלקה להנדסה ביו-רפואית

בהנחית פרופ' גילי ביסקר

אדר ה'תשפ"ה

אוניברסיטת תל – אביב

הפקולטה להנדסה ע"ש איבי ואלדר פליישמן

בית הספר לתארים מתקדמים ע"ש זנדמן-סליינר

זיהוי מתכות כבדות באמצעות ננו-צינוריות פחמן חד-שכבתיות עטופות בפפטידים המשמשות כחיישנים אופטיים

חיבור זה הוגש כעבודת גמר לקראת התואר "מוסמך אוניברסיטה" בהנדסה ביו-רפואית

על-ידי

גבריאל פטרסקי

אדר ה'תשפ"ה